iScience

CellPress
OPEN ACCESS

Article

Propagation of Pathological α-Synuclein from the Urogenital Tract to the Brain Initiates MSA-like Syndrome

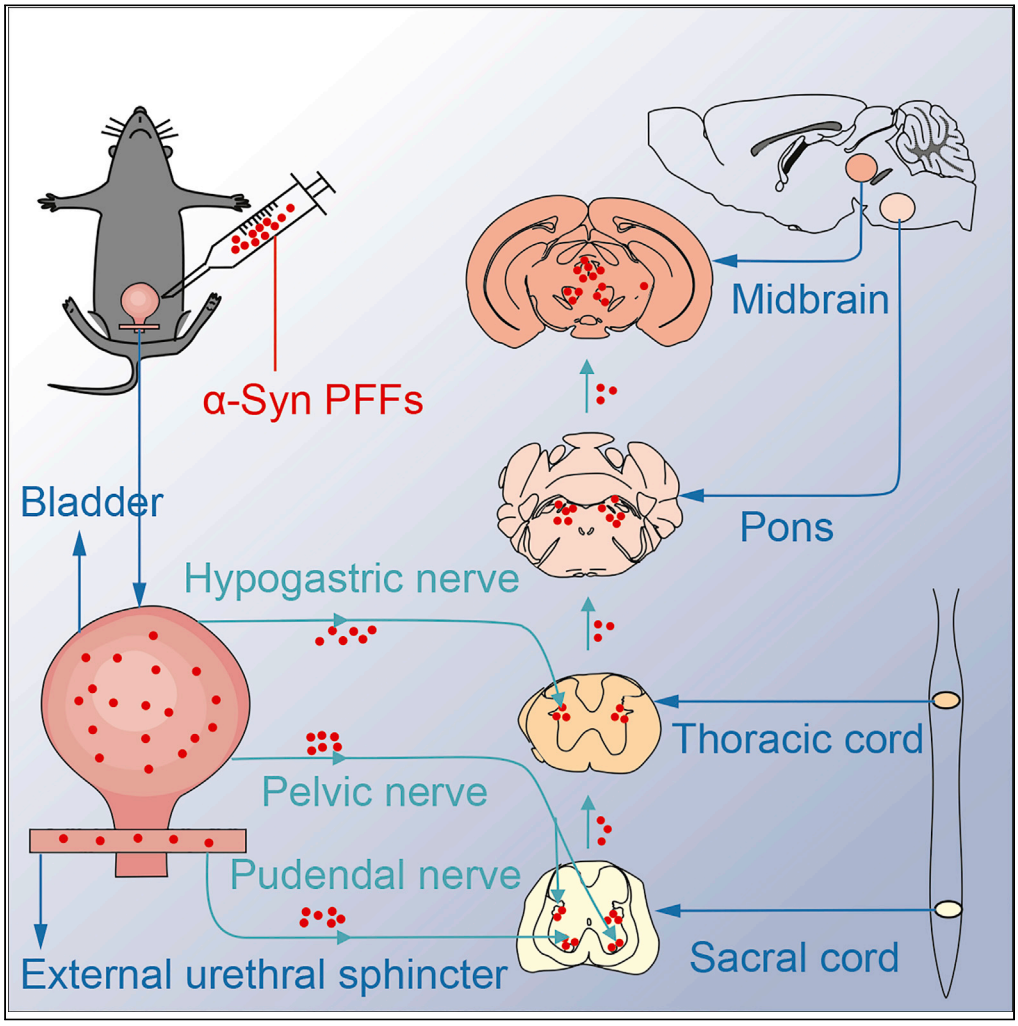

Xuebing Ding, Lebo Zhou, Xiaoyi Jiang, ..., Erxi Wu, Junfang Teng, Xuejing Wang

fccdingxb@zzu.edu.cn (X.D.)
macklon12@zzu.edu.cn (M.M.)
bstang7398@163.com (B.T.)
erxi.wu@bswhealth.org (E.W.)
13838210077@163.com (J.T.)
fccwangxj2@zzu.edu.cn (X.W.)

HIGHLIGHTS

Pathological α-Syn exhibits in nerve terminals in DET and EUS of patients with MSA

Propagation of pathological α-Syn from urinary tract to CNS causes MSA-like syndrome

The mouse models show urinary dysfunction and abnormal EAS EMG before motor deficits

Lower urinary tract injection of α-Syn PFFs induces autonomic and motor dysfunctions

Ding et al., iScience 23, 101166
June 26, 2020
https://doi.org/10.1016/j.isci.2020.101166

iScience

CellPress
OPEN ACCESS

Article

Propagation of Pathological α-Synuclein from the Urogenital Tract to the Brain Initiates MSA-like Syndrome

Xuebing Ding,[1,2,*] Lebo Zhou,[1,2] Xiaoyi Jiang,[1,2] Han Liu,[1,2] Jing Yao,[1,2] Rui Zhang,[1,2] Dongxiao Liang,[1,2] Fengfei Wang,[3,4] Mingming Ma,[5,*] Beisha Tang,[6,7,*] Erxi Wu,[3,4,8,9,*] Junfang Teng,[1,2,*] and Xuejing Wang[1,2,10,**]

SUMMARY

The neuropathological feature of multiple system atrophy (MSA), a fatal adult-onset disorder without effective therapy, is the accumulation of pathological α-synuclein (α-Syn) in the central nervous system (CNS). Here we show that pathological α-Syn exists in nerve terminals in detrusor and external urethral sphincter (EUS) of patients with MSA. Furthermore, α-Syn-preformed fibrils (PFFs) injected in the EUS or detrusor in TgM83$^{+/-}$ mice initiated the transmission of pathological α-Syn from the urogenital tract to brain via micturition reflex pathways, and these mice developed widespread phosphorylated α-Syn inclusion pathology together with phenotypes. In addition, urinary dysfunction and denervation-reinnervation of external anal sphincter were detected earlier in the mouse models with α-Syn PFFs inoculation before the behavioral manifestations. These results suggest that pathological α-Syn spreading through the micturition reflex pathways retrogradely from the urogenital tract to CNS may lead to urinary dysfunction in patients with MSA, which is different from the etiology of idiopathic Parkinson disease.

INTRODUCTION

Multiple system atrophy (MSA) is a fatal, multisystem, neurodegenerative disorder characterized by a variable combination of rapidly progressive autonomic failures, ataxia, and parkinsonism.

According to the most recent guidelines, autonomic failures featuring urogenital dysfunction, orthostatic hypotension, and respiratory disorder are premonitory symptoms and necessary for the diagnosis of MSA (Gilman et al., 2008). Retrospective data indicate that among autonomic failures, urological symptoms occur several years before the neurological symptoms in the majority of patients with MSA (Beck et al., 1994; Jecmenica-Lukic et al., 2012; Sakakibara et al., 2000). Urogenital dysfunction in patients with extrapyramidal symptoms is thought to help differentiate between Parkinson disease (PD) and MSA in early disease stages (Wenning et al., 1999). Consistently, neuropathological studies reveal that widespread pathological lesions of micturition reflex pathways, including the periaqueductal gray (PAG), Barrington nucleus (BN), intermediolateral columns (IML), Onuf nucleus of the spinal cord, and so on, are present in the central nervous system (CNS) of patients with MSA (Stemberger et al., 2010; VanderHorst et al., 2015). To date, urological deficits have been reported in the transgenic PLP-SYN mice as a transgenic mouse model of MSA (Boudes et al., 2013). However, few animal models of MSA have been established to display MSA-like urinary dysfunction and denervation-reinnervation of external anal sphincter (EAS) simultaneously.

It has been acknowledged that the cellular hallmark lesion of MSA is misfolded α-Syn accumulation within glial cytoplasmic inclusions along with neuronal inclusions (NIs) in the CNS (Woerman et al., 2018). Moreover, Watts et al. reported that brain homogenates from MSA cases induced widespread deposits of phosphorylated α-Syn (pα-Syn) in the brains of MSA-inoculated mice, and it suggested that α-Syn aggregates in the brains of MSA are transmissible but with distinct characteristics from PD (Watts et al., 2013; Yamasaki et al., 2019).

Here, we show that misfolded α-Syn exists in nerve terminals in detrusor (DET) and external urethral sphincter (EUS) of patients with MSA. To determine whether the misfolded α-Syn can induce α-Syn inclusion pathology along with autonomic failure and motor impairments by transmitting from the autonomic

[1]Department of Neurology, The First Affiliated Hospital of Zhengzhou University, Zhengzhou, Henan 450052, China

[2]Institute of Parkinson and Movement Disorder, Zhengzhou University, Zhengzhou, Henan 450052, China

[3]Neuroscience Institute and Department of Neurosurgery, Baylor Scott & White Health, Temple, TX 76508, USA

[4]College of Medicine, Texas A&M Health Science Center, College Station, TX 77843, USA

[5]Department of Neurology, Affiliated People's Hospital of Zhengzhou University, Henan Provincial People's Hospital, Zhengzhou, Henan 450003, China

[6]Department of Neurology, Xiangya Hospital, Central South University, Changsha, Hunan 410008, China

[7]National Clinical Research Center for Geriatric Disorders, Xiangya Hospital, Changsha, Hunan 410008, China

[8]College of Pharmacy, Texas A&M Health Science Center, College Station, TX 77843, USA

[9]LIVESTRONG Cancer Institutes, Dell Medical School, the University of Texas at Austin, Austin, TX 78712, USA

[10]Lead Contact

*Correspondence: fccdingxb@zzu.edu.cn (X.D.), macklon12@zzu.edu.cn (M.M.), bstang7398@163.com (B.T.), erxi.wu@bswhealth.org (E.W.), 13838210077@163.com (J.T.), fccwangxj2@zzu.edu.cn (X.W.)

https://doi.org/10.1016/j.isci.2020.101166

control of the lower urinary tract to the brain via micturition reflex pathways, we injected α-Syn preformed fibrils (PFFs) to the lower urinary tract of hemizygous TgM83$^{+/-}$ mice, and then we observed the widespread pα-Syn pathology from the autonomic control of the lower urinary tract to the brain along the micturition reflex pathways along with urinary dysfunction and motor impairments. These data provide evidence that pathological α-Syn deposited in the lower urinary tract may have the potential to induce MSA.

RESULTS

Clinical Characteristics of Patients

Forty-five patients were diagnosed as MSA, PD, or progressive supranuclear palsy (PSP) according to the consensus criteria (Gilman et al., 2008; Kalia and Lang, 2015; Litvan et al., 1996). Informed consent was obtained for each subject or their authorized surrogates on behalf of patients who lack decision-making ability. The clinical descriptions for each type of disease are summarized in Table S1. Among 32 patients (12 males and 20 females) with MSA, 13 patients had MSA with predominant parkinsonism (MSA-P), whereas 19 patients had MSA with predominant cerebellar ataxia (MSA-C). The mean ± SD of patients' ages for these two types of MSA at the time of being clinically diagnosed were 62.1 ± 7.1 years and 57.8 ± 6.6 years, respectively. The Unified Multiple System Atrophy Rating Scale (UMSARS) scores were utilized for the evaluation of patients' urological function. The score values (mean ± SD) of MSA-P and MSA-C were 44.4 ± 25.7 and 26.7 ± 15.3, respectively. In addition, these patients all had autonomic symptoms, including urological dysfunction, orthostatic dysregulation, or chronic constipation (Low et al., 2015; Stefanova et al., 2009; Wenning et al., 2004). Furthermore, the positive rates of urodynamic examination and perianal electromyography in MSA were 88.1% and 81.0%, respectively. Altogether, these data indicate that urological dysfunction is specific and common in patients with MSA.

Detection of Pathological α-Syn in Patients' Samples

We then investigated the deposits of misfolded α-Syn in the DET or EUS of patients with MSA (Figure 1J), using anti-α-Syn filament (MJFR14), anti-pα-Syn (Ser129P), and anti-aggregated-α-Syn (5G4) antibodies. Patients with MSA exhibited deposits of misfolded α-Syn in biopsy tissues (Figures 1A–1F, S1E, and S1I and Table S1). Moreover, we assessed the pathology of three sites of DET (left wall, right wall, and triangle region) by scoring the immunohistochemical pictures. For nine immunohistochemical slides (using the three antibodies to detect three sites of DET) of a patient, if more than three of five views in one slide showed α-Syn-positive staining under the microscope, one point for the slide was scored. The patients with a cumulative score (≥six points) of the whole nine slides were considered α-Syn-positive. Then, we quantified the scores of α-Syn-positive staining in MSA-P, MSA-C, PD, PSP, and normal subjects. Compared with subjects with PD or PSP or normal subjects, patients with MSA-P and MSA-C scored significantly higher ($p < 0.05$) (Figure 1I). The scores of pathological α-Syn have no significant difference between MSA-P and MSA-C ($p > 0.05$) (Figure 1I). Among the patients examined, one had a urinary incontinence for 6 years before presence of movement deficits, and we made diagnosis for him as MSA after 8 months of movement deficits. A large amount of pathological α-Syn was found in his DET and EUS. Most remarkably, no PD cases, PSP cases, or normal controls tested show pathological α-Syn in bladder (Figures 1G–1I, S1F–S1H, and S1J–S1L). Taken together, these results show that pathological α-Syn exists in DET or EUS of the patients with MSA who were examined, whereas PD, PSP, and control subjects exhibit no detectable pathological α-Syn in their bladders.

Identification of the Micturition Reflex Pathways Controlling EUS or DET Using Fluoro-Gold

After we found that misfolded α-Syn proteins exist in the DET and EUS of the detected patients, we then used fluoro-gold (FG) injection to trace the micturition reflex pathways controlling EUS or DET in mice. FG was injected into both sides of EUS or DET in TgM83$^{+/-}$ and C57BL/6 mice; the sections from different parts of nervous system were detected at 14-day post-injection. FG-labeled neurons were detected in pelvic ganglia, spinal cord, pons, and midbrain bilaterally in both mouse models (Figure S2). In spinal cord, we found that FG-labeled neurons also existed at the T2 level, which has not been previously reported. At the T2 level, the FG-labeled neurons mostly appeared in the ventral horn and IML, which are closely associated with motor and autonomic functions. Among other levels of spinal cord, FG-labeled neurons gathered in the EUS motoneurons of lamina IX (ExU9) and sacral parasympathetic nucleus (SPSy) at S1 level; EAS motoneurons of lamina IX (ExA9), ExU9, gluteal motoneurons of lamina IX (Gl9), lamina VII of the spinal gray (7Sp), and lateral spinal nucleus (LSp) at L6 level; as well as psoas motoneurons of lamina IX (Ps9), quadriceps motoneurons of lamina IX (Q9), intercalated nucleus (ICL), IML, and lumbar dorsal commissural nucleus (LDCom) at L2 level. In brain, FG-labeled neurons appeared in BN, PAG, and locus coeruleus (LC), and these nuclei have been reported to participate in micturition reflex pathways (Fowler et al., 2008). In addition, FG-labeled neurons were found to be in parvocellular reticular nucleus alpha,

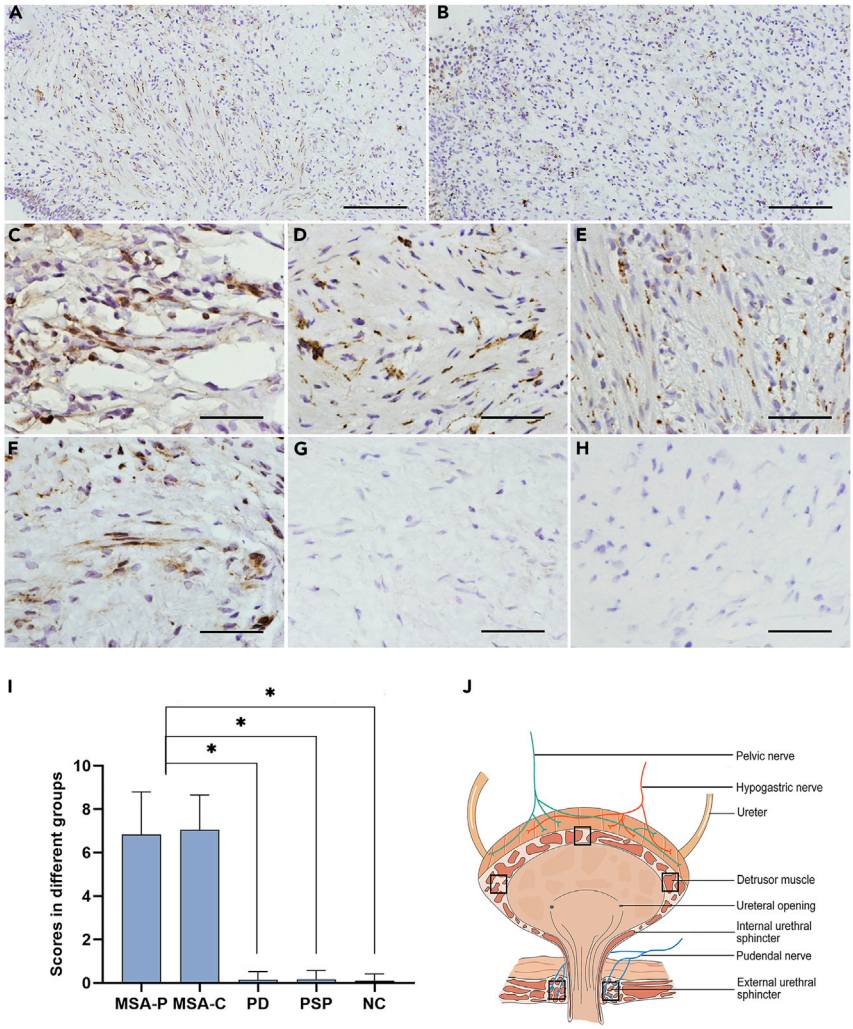

Figure 1. Immunohistochemical Results of the Sample Tissues from Different Subjects

(A–H) Representative images displayed misfolded α-Syn in DET of MSA-P (A and C–E) and MSA-C (B), and in EUS of MSA-P (F) stained with anti-α-Syn filament antibody (MJFR14), but not in PSP (G) and PD (H). (C–E) Representative images displayed the right wall of MSA-P (C), the left wall of MSA-P (D), and the triangle region of MSA-P (E).

(I) Histogram shows the scores of pathological α-Syn deposits in DET of different groups for anti-α-Syn filament (MJFR14), anti-pα-Syn (Ser129P), and anti-aggregated-α-Syn (5G4) antibodies. MSA-P, n = 13; MSA-C, n = 19; PD, n = 7; PSP, n = 6; NC, n = 20.

(J) Schematic displaying the anatomy of the lower urinary tract and sampling positions (DET and EUS).

Data are the means ± SD. Statistical significance was analyzed employing the one-way ANOVA. *p < 0.05. Scale bar, 400 μm in (A and B); 100 μm in (C–H).

mesencephalic trigeminal nucleus, and red nucleus (RN), which are involved in the general locomotion, postural control, and modulation of certain sensory and autonomic functions. Taken together, these results suggest that the micturition reflex pathways controlling EUS and DET are connected not only with the autonomic nervous system but also with the central motor pathways.

Spreading of Phosphorylated α-Syn from the Lower Urinary Tract to the Brain in TgM83$^{+/-}$ Mice via Micturition Reflex Pathways

To demonstrate whether spreading of misfolded α-Syn via the same pathways induces the MSA-like neuropathology, we next injected α-Syn PFFs to EUS or DET in TgM83$^{+/-}$ mice and evaluated pα-Syn in different sections at different time points.

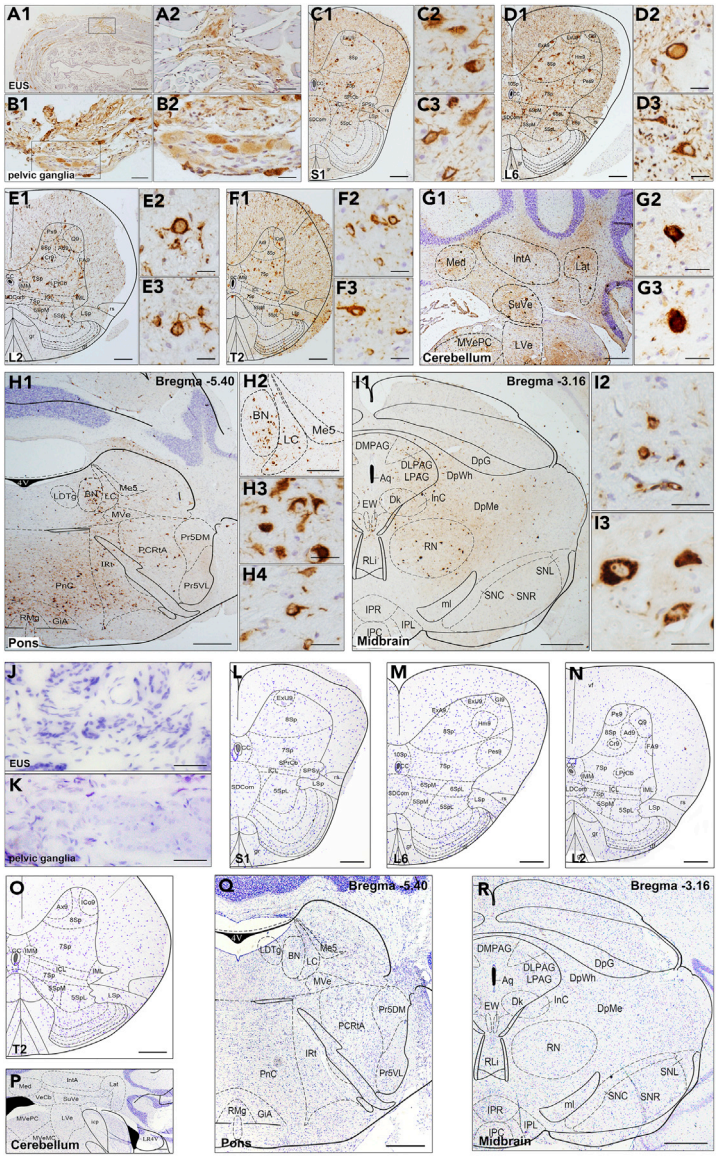
A1
A2
EUS
B1
B2
pelvic ganglia
C1
C2
C3
S1
D1
D2
D3
L6
E1
E2
E3
L2
F1
F2
F3
T2
G1
G2
G3
Med
IntA
Lat
SuVe
MVePC
LVe
Cerebellum
H1
Bregma -5.40
H2
H3
H4
BN
LC
Me5
LDTg
MVe
Pr5DM
PCRtA
IRt
PnC
Pr5VL
RMg
GiA
Pons
I1
Bregma -3.16
I2
I3
DMPAG
Aq
DLPAG
LPAG
DpG
DpWh
EW
Dk
InC
DpMe
RN
RLi
SNL
SNC
SNR
ml
IPR
IPL
IPC
Midbrain
J
K
L
M
N
O
P
Q
R
S
EUS-α-Syn PFFs TgM83+/- mice
EUS-PBS TgM83+/- mice
Mean optical density of pα-Syn-positive staining
0.5
0.4
0.3
0.2
0.1
0.0
S1
L6
L2
T2
Pons
Midbrain
Cerebellum

Figure 2. Representative Immunohistochemical Results of Different Segments from EUS-α-Syn PFFs and PBS TgM83$^{+/-}$ Mice at 6 mpi

(A–R) Pathological α-Syn was stained with anti-phospho-α-Syn (Ser 129) antibody for EUS-α-Syn PFFs TgM83$^{+/-}$ mice (A–I) and EUS-PBS TgM83$^{+/-}$ mice (J–R). Representative images displayed the distribution of pα-Syn in EUS (A1, J), pelvic ganglia (B1, K), S1 (C1, L), L6 (D1, M), L2 (E1, N), T2 (F1, O), cerebellum (G1, P), pons (H1, Q), and midbrain (I1, R). (A2–I2, C3–I3, H4) Higher-magnification views relative to the main image.

(S) Quantification of pα-Syn immunoreactivity of different segments from EUS-α-Syn PFFs and EUS-PBS TgM83$^{+/-}$ mice at 6 mpi. EUS-α-Syn PFFs TgM83$^{+/-}$ mice, n = 20; EUS-PBS TgM83$^{+/-}$ mice, n = 10.

Data are the means ± SD. Statistics were analyzed employing the Student's t test and Mann-Whitney test. *$p < 0.05$ indicates a significant difference between α-Syn PFFs groups and PBS groups. Scale bars, 500 μm in (A1, G1, H2, P); 250 μm in (C1–F1, L–O); 100 μm in (A2, B1); 50 μm in (B2, G2, I2, G3–I3, H4); 40 μm in (J, K); 25 μm in (C2–F2, C3–F3); 1 mm (H1, I1, Q, R).] DLPAG, dorsolateral periaqueductal gray; DMPAG, dorsomedial periaqueductal gray; DpG, deep gray layer of the superior colliculus; DpMe, deep mesencephalic nucleus; DpWh, deep white layer of the superior colliculus; EW, Edinger-Westphal nucleus; GiA, gigantocellular reticular nucleus; IntA, interposed cerebellar nucleus, anterior part; IPC, interpeduncular nucleus, caudal subnucleus; IPL, internal plexiform layer of the olfactory bulb; IPR, interpeduncular nucleus, rostral subnucleus; IRt, intermediate reticular nucleus; Lat, lateral (dentate) cerebellar nucleus; LDTg, tegmental nucleus; LPAG, lateral periaqueductal gray; LVe, lateral vestibular nucleus; Med, medial (fastigial) cerebellar nucleus; MVePC, medial vestibular nucleus; parvocellular part; MVe, medial vestibular nucleus; PnC, pontine reticular nucleus, caudal part; Pr5DM, principal sensory trigeminal nucleus, dorsomedial part; Pr5VL, principal sensory trigeminal nucleus, ventrolateral part; RLi, rostral linear nucleus of the raphe; RMg, raphe magnus nucleus; SuVe, superior vestibular nucleus.

Immunohistochemical results show that pα-Syn, stained with the anti-pα-Syn antibody, was detected at 5 months post-injection (mpi) in both EUS- and DET-α-Syn PFFs TgM83$^{+/-}$ mice (Figures 2A–2I, 2S). In contrast, pα-Syn has not been detected in EUS-phosphate buffer saline (PBS) (Figures 2J–2S), DET-PBS TgM83$^{+/-}$, and C57BL/6 mice post-injection. In EUS-α-Syn PFFs TgM83$^{+/-}$ mice, small numbers of pα-Syn were detected in EUS and pelvic ganglia (Figures 2A and 2B). Furthermore, pα-Syn was detected at the S1, L6, L2, and T2 levels of spinal cord, and they mostly existed in laminae V-VII and IX of these levels (Figures 2C–2F). In brain, pα-Syn existed in pons and midbrain (Figures 2H and 2I). These observations are consistent with the results of the above-mentioned FG study. In addition, using immunohistochemical approach, pα-Syn was also found in the cerebellar nuclei (Figure 2G). The diseased EUS-α-Syn PFFs TgM83$^{+/-}$ mice showed a distinct loss of calbindin-D28k and microtubule-associated protein-2 (MAP-2) (Figures 3A–3D). The number and optical density of neurons of EUS-α-Syn PFFs TgM83$^{+/-}$ mice are significantly less than PBS control groups ($p < 0.05$) (Figures 3A3–3D3). The neuropathological findings in DET-α-Syn PFFs TgM83$^{+/-}$ mice were similar to those in EUS-α-Syn PFFs TgM83$^{+/-}$ mice. In conclusion, transmission of pathological α-Syn in these mice invades not only the autonomic nervous system associated with urinary function but also the extrapyramidal system via the micturition reflex pathways, and these findings are consistent with MSA pathology found in patient autopsy (Cykowski et al., 2015; Stemberger et al., 2010; VanderHorst et al., 2015; Yoshida, 2007). Thus, these findings suggest that pathological α-Syn spreads from the autonomic innervation of the lower urinary tract to extrapyramidal system via the micturition reflex pathways, leading to widespread α-Syn pathology.

To further characterize the nature of α-Syn-positive deposits in diseased EUS- or DET-α-Syn PFFs TgM83$^{+/-}$ mice and the distribution of pathological α-Syn in various cells, double immunofluorescence staining was then employed. First, the result revealed the ubiquitin-positive pα-Syn deposits in spinal cord of diseased EUS- or DET-α-Syn PFFs TgM83$^{+/-}$ mice (Figures 3E1 and 3E3). Then, we observed the distribution of pα--Syn and Iba-1 (microglia marker) in spinal cord (Figure 3E2), which indicates that microglia are recruited around neurons containing pα-Syn. In addition, the diseased EUS-α-Syn PFFs TgM83$^{+/-}$ mice showed a distinct loss of myelin basic protein and increase of glial fibrillary acidic protein ($p < 0.05$) (Figures 3G and 3H). No pα-Syn was detected in substantia nigra pars compacta (SNc). We noticed high level of ubiquitin protein in tyrosine hydroxylase-positive dopamine neurons in SNc of both EUS- or DET-α-Syn PFFs TgM83$^{+/-}$ mice and PBS control groups (Figure 3F). Taken together, these results suggest that the injection of α-Syn PFFs into EUS or DET of TgM83$^{+/-}$ mice initiates pathological α-Syn transmission through micturition reflex pathways, which could be associated with neuronal loss, microglia recruitment, demyelination, and astrogliosis.

An immunoblot of spinal cord, pons, and PAG homogenate probed with pα-Syn (Ser129P) antibody was conducted to confirm that injection of α-Syn PFFs into EUS or DET of TgM83$^{+/-}$ mice initiates MSA-like neuropathology. In the radio immunoprecipitation assay (RIPA) buffer-insoluble and sarkosyl-insoluble fractions, immunoblots of pα-Syn reveal that bands around 15 kDa were detected in all examined diseased

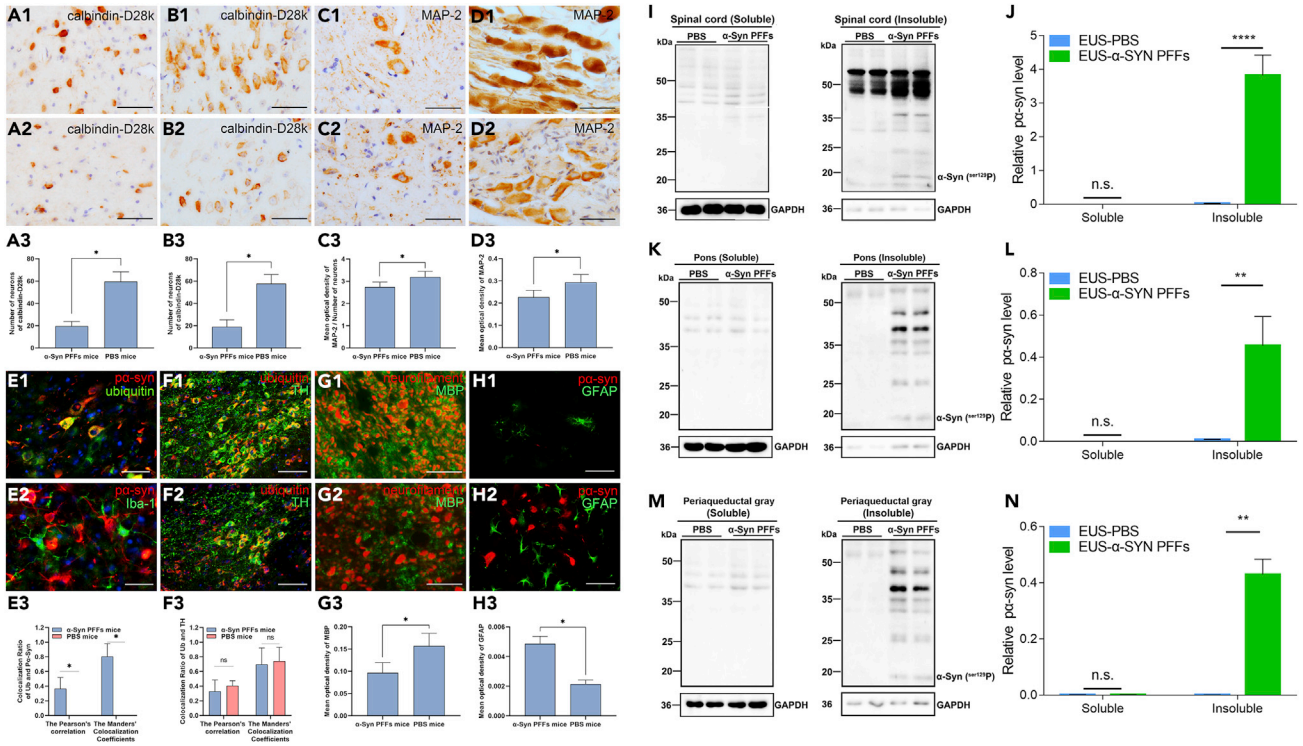

Figure 3. Immunostaining and Western Blot Analyses of Different Segments from Diseased EUS-α-Syn PFFs TgM83$^{+/-}$ Mice and Age-Matched EUS-PBS TgM83$^{+/-}$ Mice

(A–D) Immunohistochemical results from EUS-PBS TgM83$^{+/-}$ mice (A1–D1) and diseased EUS-α-Syn PFFs TgM83$^{+/-}$ mice (A2-D2) for calbindin-D28k in the periaqueductal gray (A) and Barrington nucleus (B) and MAP-2 in the intermediolateral columns of L2 (C) and pelvic ganglia (D). (A3–D3) Quantification of the number (A3, B3) and optical density (C3, D3) of neurons shown in (A1–D1 and A2–D2).

(E–H) Double immunofluorescence analysis of the L2 level of the spinal cord (E), substantia nigra (F), and pons (G, H) from EUS-PBS TgM83$^{+/-}$ mice (F1–H1) and diseased EUS-α-Syn PFFs TgM83$^{+/-}$ mice (E, F2–H2) for pα-Syn (red, E, H) with ubiquitin (Ub) (green, E1), Iba-1 (green, E2), and glial fibrillary acidic protein (GFAP) (green, H); Ub (red, F) with tyrosine hydroxylase (TH) (green, F); and neurofilament (red, G) with MBP (green, G). (E3, F3) Quantification of colocalization of Ub with pα-Syn (E3) and TH (F3) shown in (E1, F1, F2). (G3, H3) Quantification of optical density of MBP (G3) and GFAP (H3) shown in (G1, G2, H1, H2). Co-immunolabeling is represented by signal in yellow. Cell nuclei were counterstained with Hoechst 33258 (blue). EUS-α-Syn PFFs TgM83$^{+/-}$ mice, n = 20; EUS-PBS TgM83$^{+/-}$, mice n = 10. Scale bars: 200 μm in (F1, F2), 50 μm in (A1–D1, A2–D2), and 40 μm in (E1, E2, G1, G2, H1, H2).

(I–N) Representative immunoblots (I, K, M) and quantification (J, L, N) of pα-Syn in the sarkosyl-soluble and insoluble fractions of spinal cord (I, J), pons (K, L), and PAG (M, N). Blots were probed for GAPDH as a loading control (bottom). Molecular weight markers of migrated protein standards are expressed in kDa. n = 3 animals per group.

Data are the means ± SD. Statistical significance was analyzed by using the Student's t test and Mann-Whitney test, ****$p < 0.0001$, **$p < 0.01$, *$p < 0.05$; n.s., non-significant.

EUS-α-Syn TgM83$^{+/-}$ mice, whereas they were faintly detected in EUS-PBS TgM83$^{+/-}$ mice (Figures 3I–3N). Statistical analysis shows that pα-Syn is significantly increased in diseased EUS-α-Syn TgM83$^{+/-}$ mice (Figures 3J, 3L, and 3N). These data support that the injection of α-Syn PFFs into EUS or DET can induce the spreading of pathological α-Syn in CNS.

Early-Onset Denervation-Reinnervation of EAS in EUS- or DET-α-Syn PFFs TgM83$^{+/-}$

Twenty age-matched healthy TgM83$^{+/-}$ and C57BL/6 male mice were used respectively; no abnormal EAS electromyography (EMG) in these mice was detected. Based on the EMGs of the previous literature (Daube and Rubin, 2009; Palace et al., 1997; Schwarz et al., 1997), abnormal EAS EMG would be defined if the EMG findings satisfied any one of the following six conditions: (1) fibrillation potentials, (2) positive sharp waves, (3) complex repetitive discharge, (4) fasciculation potentials, (5) myokymic discharges, and (6) satellite potential.

EUS- and DET-α-Syn PFFs TgM83$^{+/-}$ mice show abnormal EAS EMGs at 2 mpi ($p < 0.05$), whereas no abnormality of EAS EMG was detected in PBS groups. Representative abnormal and normal EAS EMGs are

shown in Figures 4A–4F, respectively. The mean frequency of abnormal EAS EMGs in EUS-α-Syn PFFs TgM83$^{+/-}$ mice was 42.50%, 82.50%, and 89.00% at 2, 4, and 6 mpi, respectively, versus 41.11%, 83.89%, and 90.56% in DET-α-Syn PFFs TgM83$^{+/-}$ mice, respectively (Figure 4G). The frequency of positive sharp waves for α-Syn PFFs-injected TgM83$^{+/-}$ mice started to be significantly higher than that of PBS-injected TgM83$^{+/-}$ mice and normal control at 2 mpi (Figure 4H). In C57BL/6 mice, the data show no significant difference between EUS- or DET-α-Syn PFFs groups and PBS groups (Figures 4I and 4J). The results suggest that the frequency of abnormal EAS EMGs increases along with the progression of neural lesions caused by α-Syn PFFs. We also injected α-Syn PFFs into the intestine wall of stomach and duodenum of TgM83$^{+/-}$ mice. However, the TgM83$^{+/-}$ mice with intestine-α-Syn PFFs did not develop abnormal EAS EMG, whereas TgM83$^{+/-}$ mice did. Taken together, the denervation-reinnervation of EAS occurs in the early stage of neuropathological process in a time-dependent manner and may be caused by spreading of α-Syn PFFs from the lower urinary tract through micturition reflex pathways.

Urinary Dysfunction in EUS- or DET-α-Syn PFFs TgM83$^{+/-}$ Mice

The urodynamic baseline is determined by cystometry results of 2-month-old male TgM83$^{+/-}$ and C57BL/6 mice before treatments. Urinary dysfunction was observed in EUS- and DET-α-Syn PFFs TgM83$^{+/-}$ mice between 3 and 4 mpi and persisted to the last stage examined. At 4 mpi, both EUS- and DET-α-Syn PFFs TgM83$^{+/-}$ mice exhibited a significant increase in amplitude, postvoid residual volume (PVR), and nonvoiding contractions (NVCs) during the filling phase compared with PBS groups ($p < 0.05$). Meanwhile, voided volume (VV) and intercontraction interval (ICI) in EUS- or DET-α-Syn PFFs TgM83$^{+/-}$ mice were found less and shorter, respectively (Figure 5). The body mass of EUS- or DET-α-Syn PFFs TgM83$^{+/-}$ mice was mostly lighter than that of EUS- or DET-PBS TgM83$^{+/-}$ mice; however, the bladder of EUS- or DET-α-Syn PFFs TgM83$^{+/-}$ mice exhibited overtly greater size compared with EUS- or DET-PBS mice (Figure S3D), which was probably due to progressive urothelium and DET hyperplasia in α-Syn PFFs TgM83$^{+/-}$ mice. By 14 mpi, EUS- or DET-α-Syn PFFs C57BL/6 mice did not show any urinary dysfunction. The intestine-α-Syn PFFs TgM83$^{+/-}$ mice did not show any urinary dysfunction at 3.5 mpi even when EUS- and DET-α-Syn PFFs TgM83$^{+/-}$ mice did already. All aforementioned results suggest that urodynamic assessment in EUS- or DET-α-Syn PFFs TgM83$^{+/-}$ mice was characterized by an overactive, less-stable, and inefficient bladder. In addition, α-Syn PFFs injection into EUS or DET of TgM83$^{+/-}$ mice caused potential dyssynergia between DET and EUS, leading to hyperactive bladder and DET hyperreflexia (Boudes et al., 2013; Hamill et al., 2012), which resembles urinary dysfunction in patients with MSA. Thus, we developed an animal model to replicate MSA-like urinary disorders and abnormal EAS EMGs, which has not been previously reported.

Motor Impairments in EUS- or DET-α-Syn PFFs TgM83$^{+/-}$ Mice

Both EUS- and DET-α-Syn PFFs TgM83$^{+/-}$ mice began to exhibit motor impairments from 5 mpi. Most diseased mice presented an arched back initially and then progressed with weight loss, ataxia, paralysis, and a moribund state requiring euthanasia within 3 weeks (Figure S4A). Compared with DET-α-Syn PFFs TgM83$^{+/-}$ mice, the behavioral deficiency was more obvious in EUS-α-Syn PFFs TgM83$^{+/-}$ mice. At 5 mpi, α-Syn PFFs TgM83$^{+/-}$ mice showed significantly increased motor behavioral scale (MBS) score compared with EUS- or DET-PBS TgM83$^{+/-}$ mice, which is considered as a semi-quantitative assessment for MBS rating (Figure S4B). The rotarod test was carried out to assess coordination capability. The performance on the rotating rod was significantly impaired in EUS- and DET-α-Syn PFFs TgM83$^{+/-}$ mice compared with PBS controls, as their latency to fall was markedly reduced (Figure S4C). In an open field test, EUS- and DET-α-Syn PFFs TgM83$^{+/-}$ mice showed significantly reduced spontaneous activities when compared with PBS-injected mice (Figures S4J and S4K). Footprint analysis indicates that EUS- and DET-α-Syn PFFs TgM83$^{+/-}$ mice have shorter stride length and wider base width compared with PBS-injected mice (Figures S4D and S4E). Moreover, EUS- and DET-α-Syn PFFs TgM83$^{+/-}$ mice also showed significant motor dysfunction in the beam walking test (Figures S4F and S4G) and pole test (Figures S4H and S4I). EUS- or DET-PBS TgM83$^{+/-}$ mice did not show any phenotype until they were 22 months old, consistent with our spontaneously sick TgM83$^{+/-}$ mice in timeline. As the previous study reported, spontaneously sick TgM83$^{+/-}$ mice develop series of phenotypes between 22 and 28 months of age (Giasson et al., 2002). Nevertheless, EUS- and DET-α-Syn PFFs C57BL/6 mice failed to exhibit behavioral abnormalities up to 420 days post-injection (Figure S5).

Taken together, EUS- and DET-α-Syn PFFs TgM83$^{+/-}$ mice developed distinct motor signs including weight loss, bradykinesia, ataxia, and paralysis at 5 mpi. We conclude that injection with α-Syn PFFs into EUS or DET in TgM83$^{+/-}$ mice initiates MSA-like motor deficits.

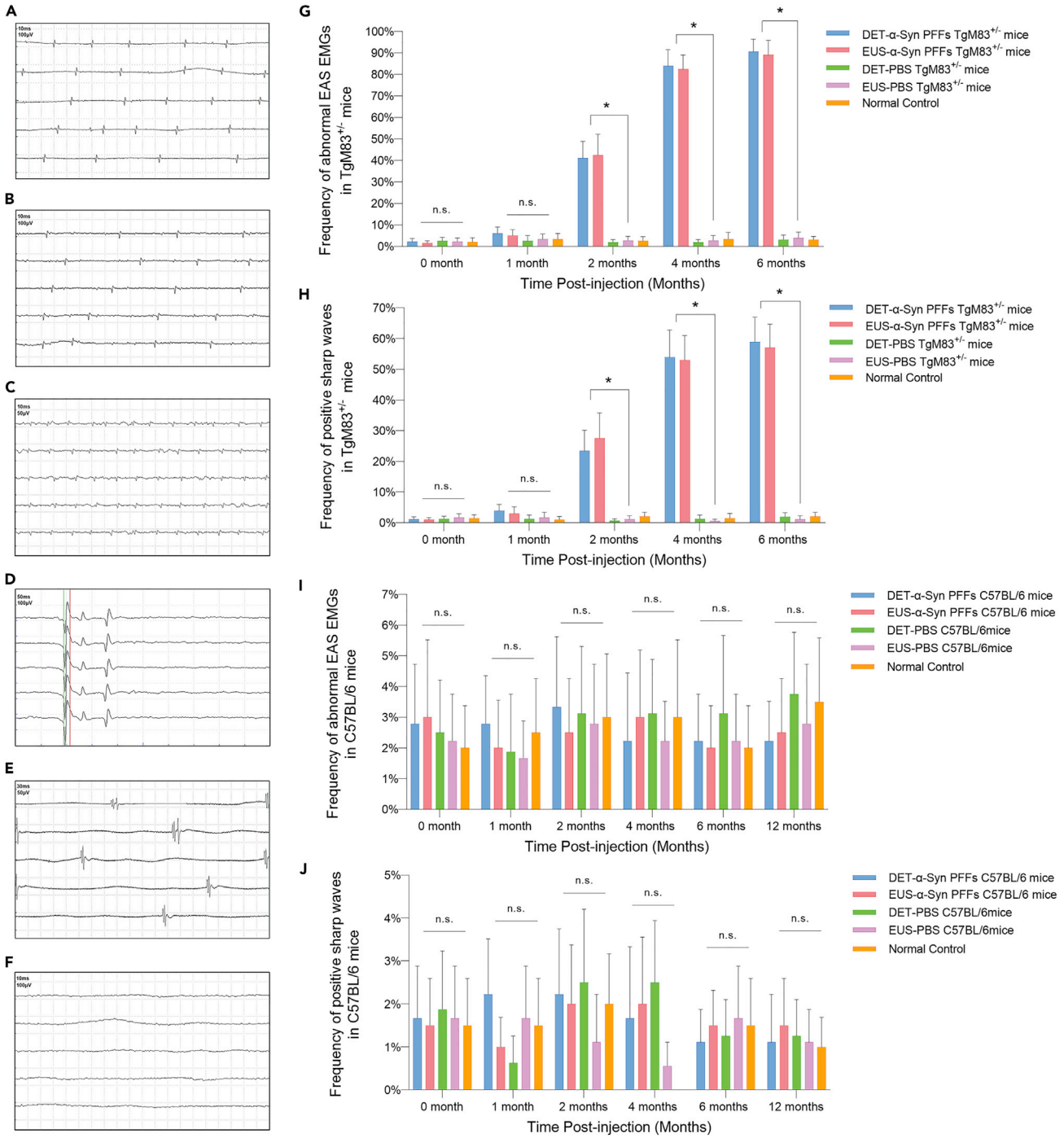

Figure 4. EAS EMG Analysis of TgM83$^{+/-}$ Mice and C57BL/6 Mice

(A–E) Representative abnormal EAS EMGs from diseased EUS- or DET-α-Syn PFFs TgM83$^{+/-}$ mice. Abnormal EAS EMGs show as fibrillation potential (A), positive sharp waves (B), complex repetitive discharge (C), satellite potential (D), and myokymic discharges (E).

(F) Representative normal EAS EMG referring to resting potential from EUS-PBS TgM83$^{+/-}$ mice at 5 mpi.

(G–J) Frequencies of abnormal EAS EMGs (G, I) and positive sharp waves (H, J) in different groups of TgM83$^{+/-}$ mice (G, H) and C57BL/6 mice (I and J). DET-α-Syn PFFs mice, n = 18; EUS-α-Syn PFFs mice, n = 20; DET-PBS mice, n = 16; EUS-PBS mice, n = 18; normal control, n = 20.

Data are the means ± SEM. Statistics was analyzed employing the one-way ANOVA. *$p < 0.05$ relative to the corresponding PBS groups and normal control groups.

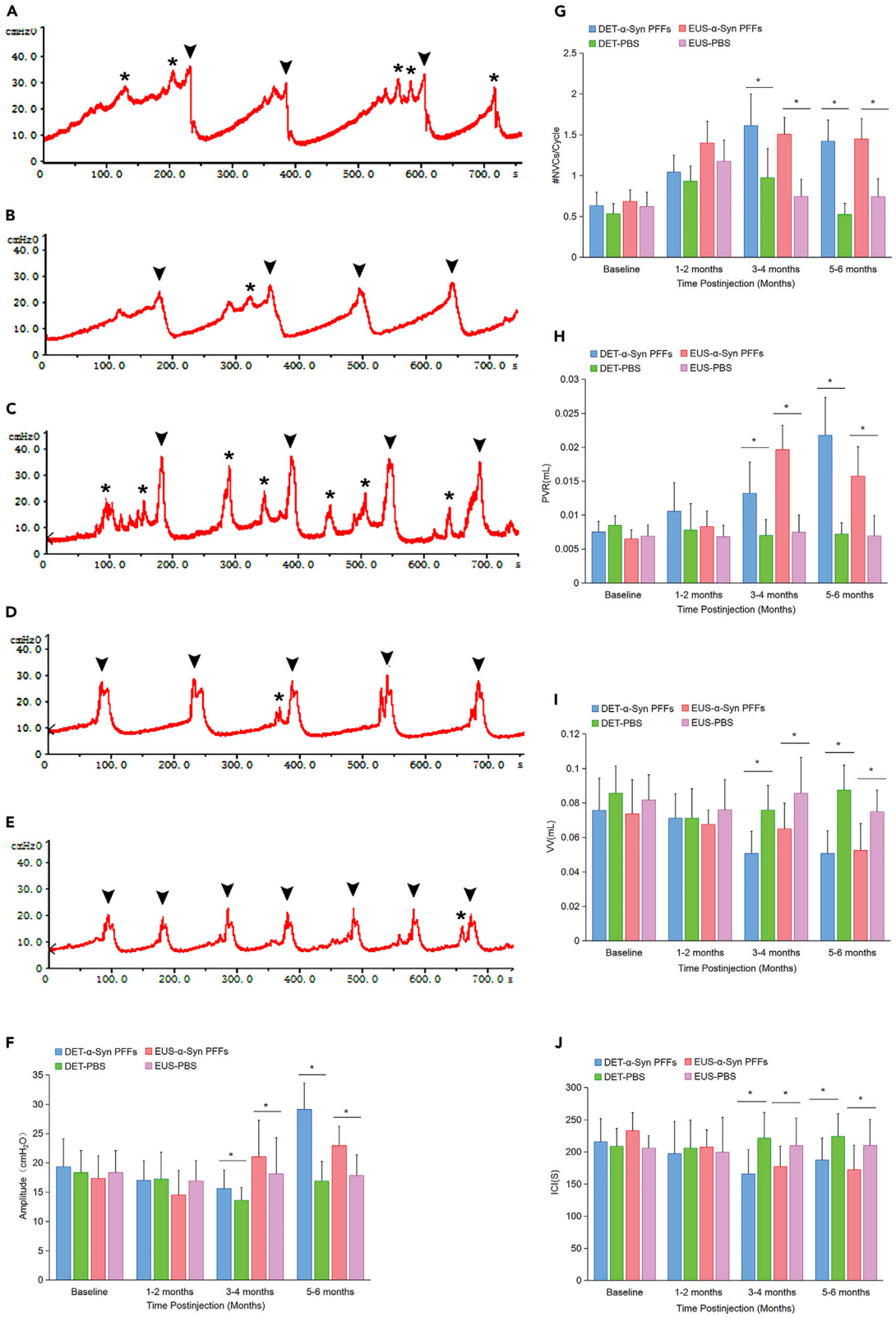
A
B
C
D
E
cmH2O
s
F
Amplitude（cmH2O）
G
#NVCs/Cycle
H
PVR(mL)
I
VV(mL)
J
ICI(S)
DET-α-Syn PFFs
EUS-α-Syn PFFs
DET-PBS
EUS-PBS
Baseline
1-2 months
3-4 months
5-6 months
Time Postinjection (Months)

Figure 5. Urinary Function Analysis of TgM83$^{+/-}$ Mice

(A–E) Representative cystometry traces in DET-α-Syn PFFs (A), DET-PBS (B), EUS-α-Syn PFFs (C), and EUS-PBS (D) TgM83$^{+/-}$ mice at 5 mpi and baseline group (E). Arrowheads indicate void events and asterisks indicate NVCs.

(F–J) Summary bar graphs from urodynamic evaluation for EUS and DET TgM83$^{+/-}$ mice including amplitude (F), #NVCs/cycle (G), PVR (H), VV (I), and ICI (J). EUS-α-Syn PFFs TgM83$^{+/-}$ mice, n = 18; DET-α-Syn PFFs TgM83$^{+/-}$ mice, n = 16; EUS-PBS TgM83$^{+/-}$ mice, n = 22; DET-PBS TgM83$^{+/-}$, mice n = 20. Data are the means ± SD. Statistics was analyzed employing the Student's t test and Mann-Whitney test. *$p < 0.05$ indicates a significant difference between EUS- or DET-α-Syn PFFs groups and EUS- or DET-PBS groups.

DISCUSSION

In MSA, autonomic dysfunctions, especially urinary dysfunction (Kirby et al., 1986), are premonitory and prominent, which are different from the other main synucleinopathies, e.g., PD. A recent review suggests that peripheral microbial infections could be potential triggers of α-synucleinopathies (Tulisiak et al., 2019). When the physiological integrity of the urinary tract is breached, the urinary tract can be at a heightened risk or even have recurrent episodes of microbial infections (Hickling et al., 2015). Based on our long-term observations of clinical subjects with these diseases, we reckoned that pathological α-Syn might exist in the lower urinary tract at the early stage of MSA instead of the gut as shown in PD (Holmqvist et al., 2014; Kim et al., 2019). To test this hypothesis, we first performed bladder biopsy in participants. The findings show that pα-Syn pathology indeed exists in DET or EUS in the included patients with MSA. The subsequent results from immunohistochemistry studies in experimental mice show that α-Syn aggregates invade the micturition reflex pathways. In addition, we found widely positive staining of pα-Syn in ventral white matter of spinal cord, possibly due to nerve tracts from brain and comprehensively longitudinal connections by synapses of numerous nerve fibers. Moreover, we detected overt pα-Syn in cerebellar nucleus, which indicates that α-Syn aggregates transmit to cerebellum via rubro-cerebello-rubrospinal circuit (Larson-Prior and Cruce, 1992). α-Syn pathology in EUS- or DET-α-Syn PFFs C57BL/6 mice was not detected at 14 mpi. The results of double immunofluorescence analysis further demonstrate the pathological lesions in the CNS of the two mouse models. There was apparent demyelination in the CNS of EUS-α-Syn PFFs TgM83$^{+/-}$ mice, which is a major pathological feature of MSA (Ettle et al., 2016; Woerman et al., 2019). The immunostaining results validate the hypothesis that pathological α-Syn transmits initially from urogenital autonomic nerves to extrapyramidal system, inducing pα-Syn pathology. EAS EMG has been previously proposed as a diagnostic method for MSA (Lee et al., 2002). Abnormalities of EAS EMG in MSA indicate the denervation-reinnervation of EAS caused by neuronal loss of Onuf nucleus in the anterior horn of the spinal cord (Lee et al., 2002; Libelius and Johansson, 2000). In this study, we conducted EAS EMG in mouse models to assess denervation-reinnervation of EAS. Remarkably, abnormal EAS EMGs emerged at 2 mpi in EUS- or DET-α-Syn PFFs TgM83$^{+/-}$ mice. Furthermore, the mean frequency reached around 90% in EUS- or DET-α-Syn PFFs TgM83$^{+/-}$ mice at 6 mpi, whereas no abnormality was detected in PBS-injected TgM83$^{+/-}$ mice. We demonstrate that EMG experimental results in the mouse models are similar to EAS EMG feature of patients with MSA preceding urinary dysfunction and movement disorders. Previous studies (Yamamoto et al., 2005) presented a view that selective neuronal loss of Onuf nucleus, which innervates EAS, results in abnormal EAS EMGs in patients with MSA. We found that pα-Syn aggregates are present in Onuf nucleus in both EUS- and DET-α-Syn PFFs TgM83$^{+/-}$ mice.

In this study, we implemented urodynamic assessment in different time points to evaluate urinary function in experimental mice. Consequently, EUS- or DET-α-Syn PFFs TgM83$^{+/-}$ mice exhibited urodynamic changes after 3 mpi, before motor impairments, versus no changes in PBS groups. Here, we identified that urinary dysfunction, characterized by urinary bladder hyperreflexia of α-Syn PFFs TgM83$^{+/-}$ mice, replicates the altered bladder function in patients with MSA including urinary incontinence, frequency, urgency, and retention (Fowler et al., 2010; Ragab and Mohammed, 2011). Previous study (Libelius and Johansson, 2000) showed that the spontaneous TgM83$^{+/-}$ mice developed urinary bladder dysfunction before motor dysfunction due to A53T mutant α-Syn. In our study, EUS- or DET-α-Syn PFFs TgM83$^{+/-}$ mice started to perform urinary dysfunction at 3.5 mpi, whereas EUS- or DET-PBS and non-inoculated TgM83$^{+/-}$ mice did not show any urinary dysfunction until they were 22 months old. The occurrence of urinary dysfunction in EUS- or DET-α-Syn PFFs TgM83$^{+/-}$ mice is earlier than that in PBS control groups and non-inoculated TgM83$^{+/-}$ mice. In our α-Syn PFFs TgM83$^{+/-}$ mice, the micturition reflex pathways, including EUS and DET, pelvic ganglia, Onuf nucleus, IML, PAG, BN, and LC, exhibited pα-Syn pathology, revealing pathological mechanisms of the urinary dysfunction. However, we did not observe appreciable levels of misfolded α-Syn deposition in oligodendrocytes within the TgM83$^{+/-}$ mice. This may be related to the transgenic background of TgM83$^{+/-}$ mice we used. As previous study reported, α-Syn in TgM83

mice is expressed under the control of the prion promoter (Giasson et al., 2002). Thus, the pathology in TgM83 mice remains essentially neuronal. This observation could be also explained by misfolded α-Syn originating from different parts of peripheral nervous system (PNS) to CNS via neuronal projections transsynaptically. In spontaneously ill TgM83$^{+/-}$ mice, α-Syn aggregates have not been detected in ExU9, ICL, ExA9, GI9, sacral dorsal commissural nucleus, IML, LDCom, BN, and PAG, which is different from the diseased EUS-α-Syn PFFs TgM83$^{+/-}$ mice. As these spared areas are involved in controlling the urinary bladder (Fowler et al., 2008), these data support that the preceding autonomic dysfunction of EUS- or DET-α-Syn PFFs TgM83$^{+/-}$ mice results from exogenously injected α-Syn PFFs instead of A53T mutant α-Syn. Besides, we injected synthetic mouse α-Syn PFFs into the EUS of C57BL/6 mice. By 6 mpi, the EUS-α-Syn PFFs C57BL/6 mice exhibited sparse pathological pα-Syn deposits at the S1, L6, L2, and T2 levels of spinal cord, and in pons and midbrain of brain (Figure S6). Moreover, they showed abnormal EAS EMG by 4 mpi and urinary dysfunction by 6 mpi (Figure S6). Together, our results suggest that misfolded α-Syn spreading through the micturition reflex pathways retrogradely may lead to urinary dysfunction.

Previous studies indicate that pathological α-Syn spreads from PNS to CNS through retrograde axonal transport, in a stereotypical and topographical pattern (Bernis et al., 2015; Braak et al., 2003; Holmqvist et al., 2014; Luk et al., 2012). Experimental studies suggest that PD pathology may originate in the vagal nerves from the gut and gradually propagate to the brain (Holmqvist et al., 2014; Kim et al., 2019). These findings support the hypothesis that different synucleinopathies may originate from different part of the PNS and gradually propagate to the CNS. Hence, we speculate that pathological α-Syn originating from the autonomic innervation of the lower urinary tract has the potential to propagate to CNS and induce MSA. Besides that, different strains of α-Syn could account for differences between α-synucleinopathies according to previous studies (Melki, 2015). Bousset et al. found that α-Syn PFFs have higher toxicity and more seeding and propagation properties compared with α-Syn ribbons (Bousset et al., 2013). Our data demonstrate that misfolded α-Syn PFFs can induce α-Syn pathology along with autonomic failure and motor impairments by transmitting from the autonomic control of the lower urinary tract to the brain via micturition reflex pathways.

As previously reported by others, peripheral injection of α-Syn PFFs into multiple sites could promote the development of α-Syn pathology in the CNS of TgM83$^{+/-}$ mice (Ayers et al., 2017; Breid et al., 2016; Holmqvist et al., 2014; Krejciova et al., 2019; Luk et al., 2012; Sacino et al., 2014a, 2014b; Watts et al., 2013; Woerman et al., 2019). We injected α-Syn PFFs into the striatum of TgM83$^{+/-}$ mice in initial studies. The results show that the lower urinary tract pathology cannot be obtained at the sixth month after intracerebral α-Syn PFFs injection. We also injected α-Syn PFFs into the intestine wall of stomach and duodenum of TgM83$^{+/-}$ mice. However, the intestine-α-Syn PFFs TgM83$^{+/-}$ mice did not develop abnormal EAS EMG and urinary dysfunction at 5 mpi when they had α-Syn pathology in the CNS and motor impairments already. Thus, α-Syn injection into intestine wall alone could not induce the denervation-reinnervation of EAS and urinary dysfunction before motor impairments in TgM83$^{+/-}$ mice. Again, this further indicates that α-Syn of PD and MSA may start in different places.

Here we further show that injection with α-Syn PFFs into EUS or DET induces a rapid progression of motor dysfunctions. Our study shows that injection with α-Syn PFFs into EUS or DET in TgM83$^{+/-}$ mice causes not only seeding of α-Syn aggregation in the CNS but also rapid progressive motor dysfunctions evaluated using a spectrum of behavioral tests. From our findings, the occurrence of motor impairments in our EUS- or DET-α-Syn PFFs TgM83$^{+/-}$ mice was much earlier than spontaneously ill TgM83$^{+/-}$ mice (Giasson et al., 2002). According to previous studies (Breid et al., 2016; Holmqvist et al., 2014; Prusiner et al., 2015; Sacino et al., 2014a, 2014b), the animal models of synucleinopathy induced by exogenous inoculation involve different inocula and inoculation positions, developing variable α-Syn pathology and motor impairments without autonomic dysfunction. Furthermore, pathology of α-Syn inclusions observed in motor neuron of ventral horn, cerebellum, and RN in α-Syn PFFs TgM83$^{+/-}$ mice provides neuropathological evidence for the motor impairments.

In summary, we observe that pathological α-Syn exists in nerve terminals in DET and EUS of patients with MSA, which has not been recognized before. Also, this study suggests one possible pathogenic mechanism of MSA, which is the spreading of α-Syn pathology from the autonomic control of the lower urinary tract to the brain. Finally, our data support the view that pathological α-Syn may originate from different

parts of PNS among different disorders of synucleinopathies. However, the full mechanisms of MSA warrant further explanation as other possibilities exist at the same time.

Limitations of the Study

MSA is a sporadic disease rather than a genetic disease; the conclusions accordingly are constrained by the transgenic mice used for the research, and further investigation on wild-type mice might provide more evidence. In addition, the essentially neuronal pathology and the absence of oligodendroglial inclusion in TgM83$^{+/-}$ mice may provide an imperfect model for MSA.

Resource Availability

Lead Contact

Further information and requests for resources should be directed to and will be fulfilled by the Lead Contact, Xuejing Wang (fccwangxj2@zzu.edu.cn).

Materials Availability

All unique/stable reagents generated in this study are available from the Lead Contact with a completed Materials Transfer Agreement.

Data and Code Availability

All data supporting the findings of this study are included in the article and its Supplemental Information, or are available from the corresponding authors on request.

METHODS

All methods can be found in the accompanying Transparent Methods supplemental file.

SUPPLEMENTAL INFORMATION

Supplemental Information can be found online at https://doi.org/10.1016/j.isci.2020.101166.

ACKNOWLEDGMENTS

We thank all our collaborators at the First Affiliated Hospital of Zhengzhou University for their assistance with patient sample collection. Specially, we thank Dr. Jianping Wang for his material support and Dr. Shuyan Feng for her excellent technical support. This work was supported by National Natural Science Foundation of China (No. 81873791, 81471307) to X.W.; Natural Science Foundation of Henan Province of China (182300410373) to X.D.; National Natural Science Foundation of China (No. 81671267) and Natural Science Foundation of Henan Province of China (182300410320) to J.T.; and Baylor Scott & White Health Funds to E.W.

AUTHOR CONTRIBUTIONS

X.W. and X.D. designed the study; X.W., J.T., and M.M. organized the research project; L.Z., X.J., H.L., J.Y., R.Z., and D.L. conducted the experiments; E.W. and M.M. designed the statistical analysis; X.D., F.W., and X.J. executed the statistical analysis; X.W., J.T., and B.T. did review and critique of the statistical analysis; X.W. wrote the first draft; E.W., L.Z., and H.L. did review and critique of the manuscript.

DECLARATION OF INTERESTS

The authors declare no competing interests.

Received: July 17, 2019
Revised: December 29, 2019
Accepted: May 8, 2020
Published: June 26, 2020

REFERENCES

Ayers, J.I., Brooks, M.M., Rutherford, N.J., Howard, J.K., Sorrentino, Z.A., Riffe, C.J., and Giasson, B.I. (2017). Robust central nervous system pathology in transgenic mice following peripheral injection of alpha-synuclein fibrils. J. Virol. *91*, e02095–16.

Beck, R.O., Betts, C.D., and Fowler, C.J. (1994). Genitourinary dysfunction in multiple system atrophy: clinical features and treatment in 62 cases. J. Urol. *151*, 1336–1341.

Bernis, M.E., Babila, J.T., Breid, S., Wusten, K.A., Wullner, U., and Tamguney, G. (2015). Prion-like propagation of human brain-derived alpha-synuclein in transgenic mice expressing human wild-type alpha-synuclein. Acta Neuropathol. Commun. *3*, 75.

Boudes, M., Uvin, P., Pinto, S., Voets, T., Fowler, C.J., Wenning, G.K., De Ridder, D., and Stefanova, N. (2013). Bladder dysfunction in a transgenic mouse model of multiple system atrophy. Mov. Disord. *28*, 347–355.

Bousset, L., Pieri, L., Ruiz-Arlandis, G., Gath, J., Jensen, P.H., Habenstein, B., Madiona, K., Olieric, V., Bockmann, A., Meier, B.H., et al. (2013). Structural and functional characterization of two alpha-synuclein strains. Nat. Commun. *4*, 2575.

Braak, H., Del Tredici, K., Rub, U., de Vos, R.A., Jansen Steur, E.N., and Braak, E. (2003). Staging of brain pathology related to sporadic Parkinson's disease. Neurobiol. Aging *24*, 197–211.

Breid, S., Bernis, M.E., Babila, J.T., Garza, M.C., Wille, H., and Tamguney, G. (2016). Neuroinvasion of alpha-synuclein prionoids after intraperitoneal and intraglossal inoculation. J. Virol. *90*, 9182–9193.

Cykowski, M.D., Coon, E.A., Powell, S.Z., Jenkins, S.M., Benarroch, E.E., Low, P.A., Schmeichel, A.M., and Parisi, J.E. (2015). Expanding the spectrum of neuronal pathology in multiple system atrophy. Brain. *138*, 2293–2309.

Daube, J.R., and Rubin, D.I. (2009). Needle electromyography. Muscle Nerve *39*, 244–270.

Ettle, B., Kerman, B.E., Valera, E., Gillmann, C., Schlachetzki, J.C., Reiprich, S., Buttner, C., Ekici, A.B., Reis, A., Wegner, M., et al. (2016). alpha-Synuclein-induced myelination deficit defines a novel interventional target for multiple system atrophy. Acta Neuropathol. *132*, 59–75.

Fowler, C.J., Dalton, C., and Panicker, J.N. (2010). Review of neurologic diseases for the urologist. Urol. Clin. North Am. *37*, 517–526.

Fowler, C.J., Griffiths, D., and de Groat, W.C. (2008). The neural control of micturition. Nat. Rev. Neurosci. *9*, 453–466.

Giasson, B.I., Duda, J.E., Quinn, S.M., Zhang, B., Trojanowski, J.Q., and Lee, V.M. (2002). Neuronal alpha-synucleinopathy with severe movement disorder in mice expressing A53T human alpha-synuclein. Neuron *34*, 521–533.

Gilman, S., Wenning, G.K., Low, P.A., Brooks, D.J., Mathias, C.J., Trojanowski, J.Q., Wood, N.W., Colosimo, C., Durr, A., Fowler, C.J., et al. (2008). Second consensus statement on the diagnosis of multiple system atrophy. Neurology *71*, 670–676.

Hamill, R.W., Tompkins, J.D., Girard, B.M., Kershen, R.T., Parsons, R.L., and Vizzard, M.A. (2012). Autonomic dysfunction and plasticity in micturition reflexes in human alpha-synuclein mice. Dev. Neurobiol. *72*, 918–936.

Hickling, D.R., Sun, T.T., and Wu, X.R. (2015). Anatomy and physiology of the urinary tract: relation to host defense and microbial infection. Microbiol. Spectr. *3*, 10.1128.

Holmqvist, S., Chutna, O., Bousset, L., Aldrin-Kirk, P., Li, W., Bjorklund, T., Wang, Z.Y., Roybon, L., Melki, R., and Li, J.Y. (2014). Direct evidence of Parkinson pathology spread from the gastrointestinal tract to the brain in rats. Acta Neuropathol. *128*, 805–820.

Jecmenica-Lukic, M., Poewe, W., Tolosa, E., and Wenning, G.K. (2012). Premotor signs and symptoms of multiple system atrophy. Lancet Neurol. *11*, 361–368.

Kalia, L.V., and Lang, A.E. (2015). Parkinson's disease. Lancet *386*, 896–912.

Kim, S., Kwon, S.H., Kam, T.I., Panicker, N., Karuppagounder, S.S., Lee, S., Lee, J.H., Kim, W.R., Kook, M., Foss, C.A., et al. (2019). Transneuronal propagation of pathologic alpha-synuclein from the gut to the brain models Parkinson's disease. Neuron *103*, 627–641.e7.

Kirby, R., Fowler, C., Gosling, J., and Bannister, R. (1986). Urethro-vesical dysfunction in progressive autonomic failure with multiple system atrophy. J. Neurol. Neurosurg. Psychiatry *49*, 554–562.

Krejciova, Z., Carlson, G.A., Giles, K., and Prusiner, S.B. (2019). Replication of multiple system atrophy prions in primary astrocyte cultures from transgenic mice expressing human alpha-synuclein. Acta Neuropathol. Commun. *7*, 81.

Larson-Prior, L.J., and Cruce, W.L. (1992). The red nucleus and mesencephalic tegmentum in a ranid amphibian: a cytoarchitectonic and HRP connectional study. Brain Behav. Evol. *40*, 273–286.

Lee, E.A., Kim, B.J., and Lee, W.Y. (2002). Diagnosing multiple system atrophy with greater accuracy: combined analysis of the clonidine-growth hormone test and external anal sphincter electromyography. Mov. Disord. *17*, 1242–1247.

Libelius, R., and Johansson, F. (2000). Quantitative electromyography of the external anal sphincter in Parkinson's disease and multiple system atrophy. Muscle Nerve *23*, 1250–1256.

Litvan, I., Agid, Y., Calne, D., Campbell, G., Dubois, B., Duvoisin, R.C., Goetz, C.G., Golbe, L.I., Grafman, J., Growdon, J.H., et al. (1996). Clinical research criteria for the diagnosis of progressive supranuclear palsy (Steele-Richardson-Olszewski syndrome): report of the NINDS-SPSP international workshop. Neurology *47*, 1–9.

Low, P.A., Reich, S.G., Jankovic, J., Shults, C.W., Stern, M.B., Novak, P., Tanner, C.M., Gilman, S., Marshall, F.J., Wooten, F., et al. (2015). Natural history of multiple system atrophy in the USA: a prospective cohort study. Lancet Neurol. *14*, 710–719.

Luk, K.C., Kehm, V., Carroll, J., Zhang, B., O'Brien, P., Trojanowski, J.Q., and Lee, V.M. (2012). Pathological alpha-synuclein transmission initiates Parkinson-like neurodegeneration in nontransgenic mice. Science *338*, 949–953.

Melki, R. (2015). Role of different alpha-synuclein strains in synucleinopathies, similarities with other neurodegenerative diseases. J. Parkinsons Dis. *5*, 217–227.

Palace, J., Chandiramani, V.A., and Fowler, C.J. (1997). Value of sphincter electromyography in the diagnosis of multiple system atrophy. Muscle Nerve *20*, 1396–1403.

Prusiner, S.B., Woerman, A.L., Mordes, D.A., Watts, J.C., Rampersaud, R., Berry, D.B., Patel, S., Oehler, A., Lowe, J.K., Kravitz, S.N., et al. (2015). Evidence for alpha-synuclein prions causing multiple system atrophy in humans with parkinsonism. Proc. Natl. Acad. Sci. U S A *112*, E5308–E5317.

Ragab, M.M., and Mohammed, E.S. (2011). Idiopathic Parkinson's disease patients at the urologic clinic. Neurourol Urodyn. *30*, 1258–1261.

Sacino, A.N., Brooks, M., Thomas, M.A., McKinney, A.B., Lee, S., Regenhardt, R.W., McGarvey, N.H., Ayers, J.I., Notterpek, L., Borchelt, D.R., et al. (2014a). Intramuscular injection of alpha-synuclein induces CNS alpha-synuclein pathology and a rapid-onset motor phenotype in transgenic mice. Proc. Natl. Acad. Sci. U S A *111*, 10732–10737.

Sacino, A.N., Brooks, M., Thomas, M.A., McKinney, A.B., McGarvey, N.H., Rutherford, N.J., Ceballos-Diaz, C., Robertson, J., Golde, T.E., and Giasson, B.I. (2014b). Amyloidogenic alpha-synuclein seeds do not invariably induce rapid, widespread pathology in mice. Acta Neuropathol. *127*, 645–665.

Sakakibara, R., Hattori, T., Uchiyama, T., Kita, K., Asahina, M., Suzuki, A., and Yamanishi, T. (2000). Urinary dysfunction and orthostatic hypotension in multiple system atrophy: which is the more common and earlier manifestation? J. Neurol. Neurosurg. Psychiatry *68*, 65–69.

Schwarz, J., Kornhuber, M., Bischoff, C., and Straube, A. (1997). Electromyography of the external anal sphincter in patients with Parkinson's disease and multiple system atrophy: frequency of abnormal spontaneous activity and polyphasic motor unit potentials. Muscle Nerve *20*, 1167–1172.

Stefanova, N., Bucke, P., Duerr, S., and Wenning, G.K. (2009). Multiple system atrophy: an update. Lancet Neurol. *8*, 1172–1178.

Stemberger, S., Poewe, W., Wenning, G.K., and Stefanova, N. (2010). Targeted overexpression of human alpha-synuclein in oligodendroglia induces lesions linked to MSA-like progressive autonomic failure. Exp. Neurol. *224*, 459–464.

Tulisiak, C.T., Mercado, G., Peelaerts, W., Brundin, L., and Brundin, P. (2019). Can infections

trigger alpha-synucleinopathies? Prog. Mol. Biol. Transl. Sci. *168*, 299–322.

VanderHorst, V.G., Samardzic, T., Saper, C.B., Anderson, M.P., Nag, S., Schneider, J.A., Bennett, D.A., and Buchman, A.S. (2015). alpha-Synuclein pathology accumulates in sacral spinal visceral sensory pathways. Ann. Neurol. *78*, 142–149.

Watts, J.C., Giles, K., Oehler, A., Middleton, L., Dexter, D.T., Gentleman, S.M., DeArmond, S.J., and Prusiner, S.B. (2013). Transmission of multiple system atrophy prions to transgenic mice. Proc. Natl. Acad. Sci. U S A *110*, 19555–19560.

Wenning, G.K., Scherfler, C., Granata, R., Bosch, S., Verny, M., Chaudhuri, K.R., Jellinger, K., Poewe, W., and Litvan, I. (1999). Time course of symptomatic orthostatic hypotension and urinary incontinence in patients with postmortem confirmed parkinsonian syndromes: a clinicopathological study. J. Neurol. Neurosurg. Psychiatry *67*, 620–623.

Wenning, G.K., Tison, F., Seppi, K., Sampaio, C., Diem, A., Yekhlef, F., Ghorayeb, I., Ory, F., Galitzky, M., Scaravilli, T., et al. (2004). Development and validation of the unified multiple system Atrophy rating scale (UMSARS). Mov. Disord. *19*, 1391–1402.

Woerman, A.L., Oehler, A., Kazmi, S.A., Lee, J., Halliday, G.M., Middleton, L.T., Gentleman, S.M., Mordes, D.A., Spina, S., Grinberg, L.T., et al. (2019). Multiple system atrophy prions retain strain specificity after serial propagation in two different Tg(SNCA*A53T) mouse lines. Acta Neuropathol. *137*, 437–454.

Woerman, A.L., Watts, J.C., Aoyagi, A., Giles, K., Middleton, L.T., and Prusiner, S.B. (2018). Alpha-synuclein: multiple system Atrophy prions. Cold Spring Harb. Perspect. Med. *8*, a024588.

Yamamoto, T., Sakakibara, R., Uchiyama, T., Liu, Z., Ito, T., Awa, Y., Yamamoto, K., Kinou, M., Yamanishi, T., and Hattori, T. (2005). When is Onuf's nucleus involved in multiple system atrophy? A sphincter electromyography study. J. Neurol. Neurosurg. Psychiatry *76*, 1645–1648.

Yamasaki, T.R., Holmes, B.B., Furman, J.L., Dhavale, D.D., Su, B.W., Song, E.S., Cairns, N.J., Kotzbauer, P.T., and Diamond, M.I. (2019). Parkinson's disease and multiple system atrophy have distinct alpha-synuclein seed characteristics. J. Biol. Chem. *294*, 1045–1058.

Yoshida, M. (2007). Multiple system atrophy: alpha-synuclein and neuronal degeneration. Neuropathology *27*, 484–493.

iScience, Volume *23*

Supplemental Information

Propagation of Pathological α-Synuclein from the Urogenital Tract to the Brain Initiates MSA-like Syndrome

Xuebing Ding, Lebo Zhou, Xiaoyi Jiang, Han Liu, Jing Yao, Rui Zhang, Dongxiao Liang, Fengfei Wang, Mingming Ma, Beisha Tang, Erxi Wu, Junfang Teng, and Xuejing Wang

Supplemental Figures

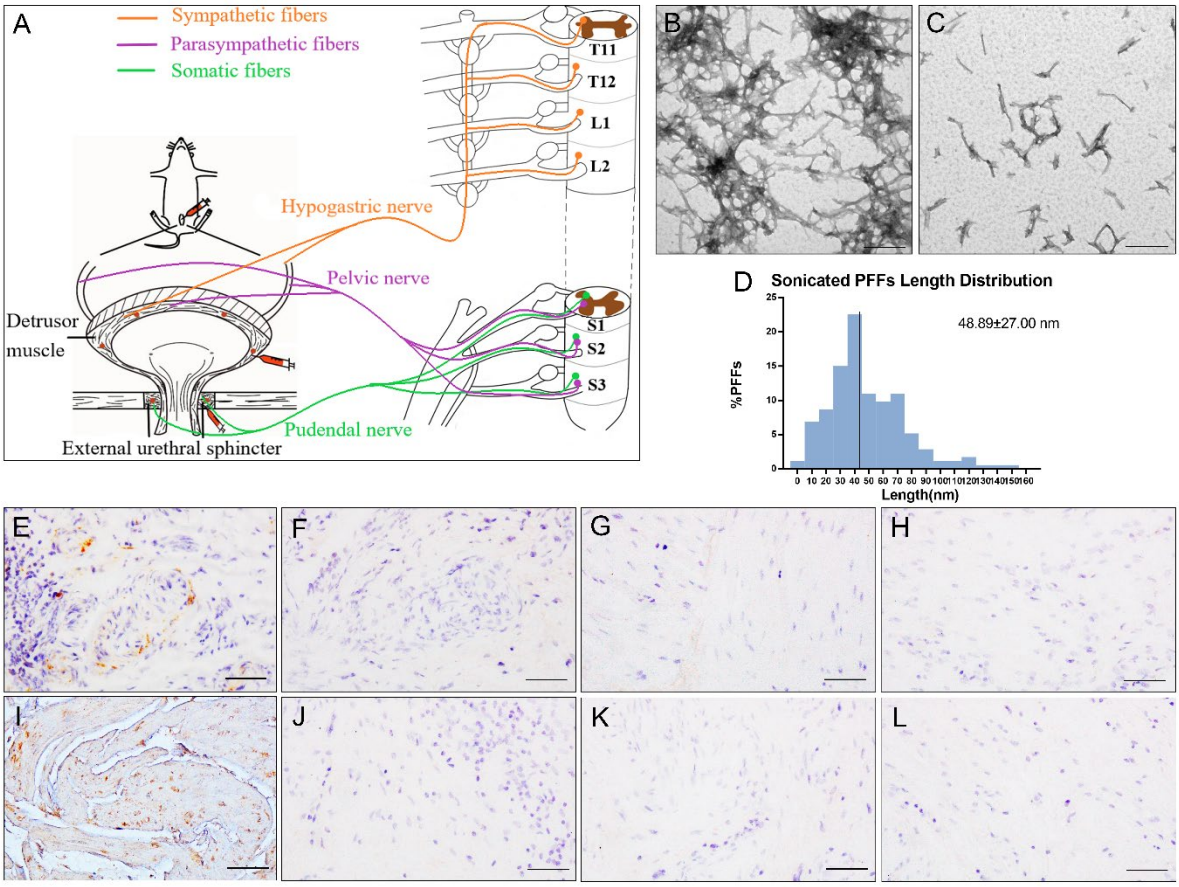

Figure S1. Related to Figure 1 and Transparent Methods. (A) Schematic displaying the innervation of the EUS and DET by the hypogastric, pelvic, and pudendal nerves. (B, C) Representative negative-stained transmission electron micrographs of α-Syn PFFs before sonication (B) and after sonication (C). (D) Histogram representation of >170 sonicated fibrils measured from randomly captured electron microscopy images. Black bars represent group median, with mean and corresponding group standard deviation indicated in bold font. (E-L) Representative immunohistochemical images of DET from MSA (E, I), PD (F, J), PSP (G, K) and NC (H, L) using anti-pα-Syn (Ser129) (E-H) and anti-α-Syn aggregates (5G4) (I-L) antibodies. [Scale bars, 500 nm (B, C); 100 μm (E-L).]

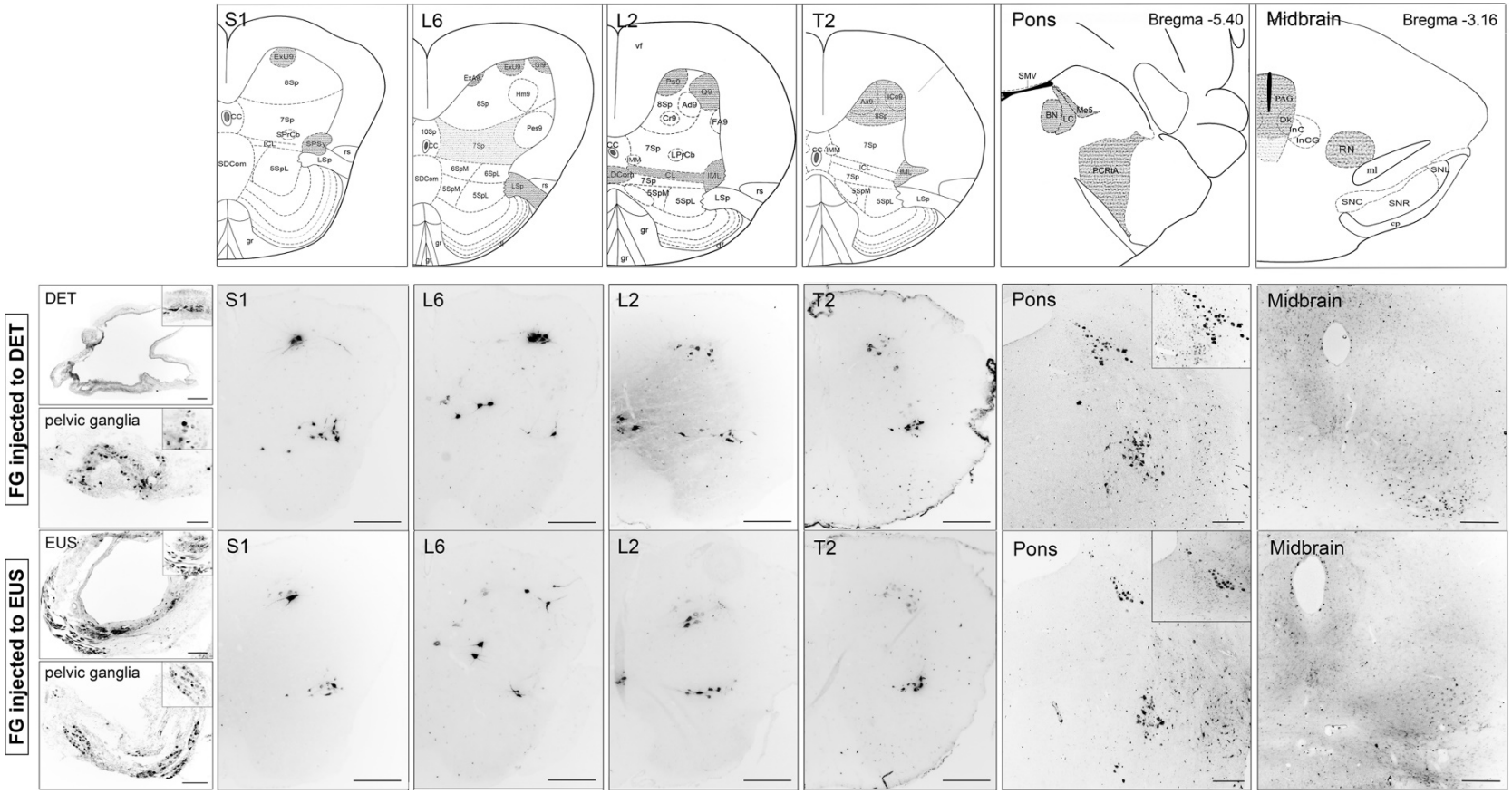
S1
L6
L2
T2
Pons
Bregma -5.40
Midbrain
Bregma -3.16
FG injected to DET
FG injected to EUS
DET
EUS
pelvic ganglia
pelvic ganglia

Figure S2. Representative images of FG-labeled neurons in DET- and EUS-FG C57BL/6 mice. Related to Figure 2. All FG-labeled neurons appeared bilaterally while displayed one side. Schematics in the upper panel displayed the map of retrograde tracing areas (shaded areas) at different levels. Labeling appeared in DET-FG C57BL/6 mice (middle panel) and EUS-FG C57BL/6 mice (lower panel). Insets show a higher magnification relative to the main image. [Scale bars, 200 μm (DET, EUS, pons); 100 μm (pelvic ganglia); 500 μm (S1, L6, L2, T2, midbrain).] Abbreviation: 5SpL: lamina V of the spinal gray, lateral part; 5SpM: lamina V of the spinal gray, medial part; 6SpL: lamina Ⅵ of the spinal gray, lateral part; 6SpM: lamina Ⅵ of the spinal gray, medial part; 7Sp: lamina Ⅶ of the spinal gray; 8Sp: lamina Ⅷ of the spinal gray; 10Sp: lamina Ⅹ of the spinal gray; Ad9: adductor motoneurons of lamina Ⅸ; Ax9: axial muscle motoneurons of lamina Ⅸ; BN: Barrington's nucleus; CC: central canal; cp: cerebral peduncle, basal part; Cr9: cremaster motoneurons of lamina Ⅸ; csc: commissure of the superior colliculus; DET: detrusor; df: dorsal funiculus; Dk: nucleus of Darkschewitsch; dl: dorsolateral fasciculus (Lissauer); ExA9: external anal sphincter motoneurons of lamina IX; ExU9: external urethral sphincter motoneurons of lamina IX; EUS: external urethral sphincter; FG: Fluoro-Gold; Gl9: gluteal motoneurons of lamina IX; gr: gracile fasciculus; Hm9: hamstring motoneurons of lamina Ⅸ; ICL: intercalated nucleus; ICo9: intercostal muscle motoneurons of lamina Ⅸ; IML: intermediolateral columns; IMM: intermediomedial column; InCG: interstitial nucleus of Cajal, greater part; InC: interstitial nucleus of Cajal; LC: locus coeruleus; LDCom: lumbar dorsal commissural nucleus; LPrCb: lumbar precerebellar nucleus; LSp: lateral spinal nucleus; Me5: mesencephalic trigeminal nucleus; ml: medial lemniscus; PAG: periaqueductal gray; PCRtA: parvocellular reticular nucleus alpha; Pes9: pes motoneurons of lamina Ⅸ; Ps9: psoas motoneurons of lamina IX; Q9: quadriceps motoneurons of lamina IX; RN: red nucleus; rs: rubrospinal tract; SDCom: sacral dorsal commissural nucleus; SMV: superior medullary velum; SNC: substantia nigra pars compacta; SNL: substantia nigra, lateral part; SNR: substantia nigra, reticular part; SPrCb: sacral precerebellar nucleus; SPSy: sacral parasympathetic nucleus; vf: ventral funiculus.

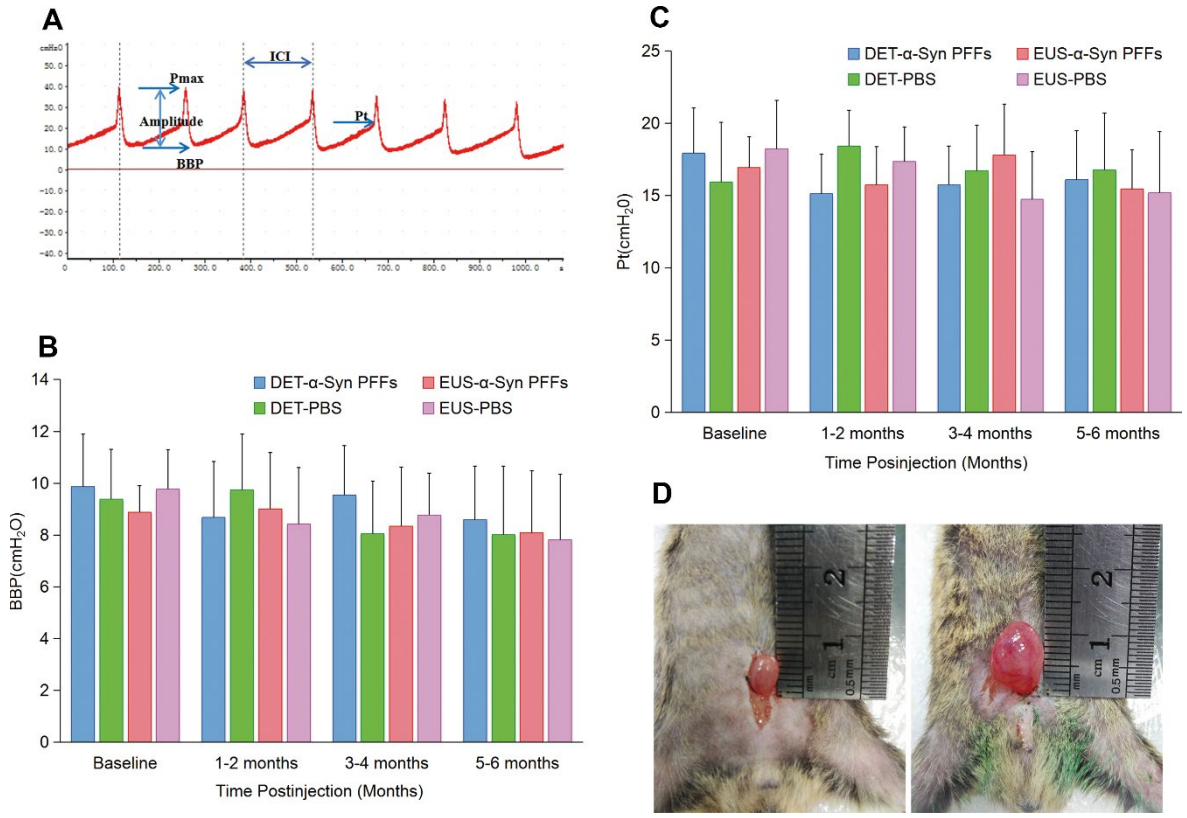

Figure S3. Urinary function analysis. Related to Figure 5. (A) Representative cystometric curve of normal C57BL/6 mice. (B and C) Summary bar graphs from urodynamic evaluation about BBP (B) and Pt (C) for EUS and DET TgM83$^{+/-}$ mice. EUS-α-Syn PFFs TgM83$^{+/-}$ mice n = 18, DET-α-Syn PFFs TgM83$^{+/-}$ mice n = 16, EUS-PBS TgM83$^{+/-}$ mice n = 22, DET-PBS TgM83$^{+/-}$ mice n = 20. Data are the means ± SD. Statistics was performed employing the Student's t test and Mann-Whitney test. (D) Bladder size of EUS-α-Syn PFFs (right) and EUS-PBS (left) TgM83$^{+/-}$ mice at 6-month post-injection (mpi).

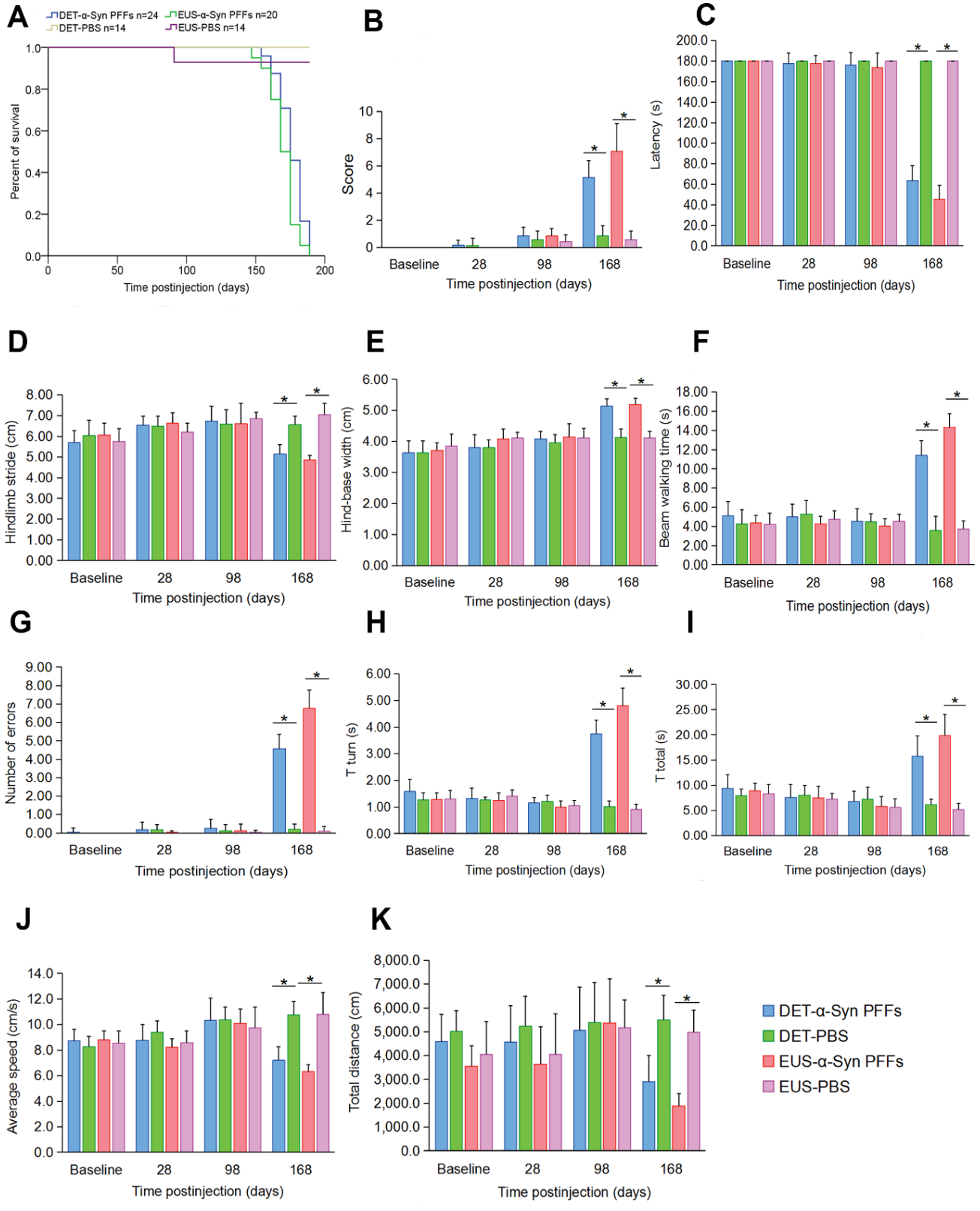
A
DET-α-Syn PFFs n=24
EUS-α-Syn PFFs n=20
DET-PBS n=14
EUS-PBS n=14
Percent of survival
Time postinjection (days)
B
Score
Baseline
28
98
168
Time postinjection (days)
C
Latency (s)
Time postinjection (days)
D
Hindlimb stride (cm)
Time postinjection (days)
E
Hind-base width (cm)
Time postinjection (days)
F
Beam walking time (s)
Time postinjection (days)
G
Number of errors
Time postinjection (days)
H
T turn (s)
Time postinjection (days)
I
T total (s)
Time postinjection (days)
J
Average speed (cm/s)
Time postinjection (days)
K
Total distance (cm)
Time postinjection (days)
DET-α-Syn PFFs
DET-PBS
EUS-α-Syn PFFs
EUS-PBS

Figure S4. Behavioral analysis of TgM83$^{+/-}$ mice. Related to Figure 4 and 5. (A) Kaplan-Meier survival plot shows decreased survival time (due to death or euthanasia because of paralysis) for α-Syn PFFs TgM83$^{+/-}$ mice compared with age-matched PBS TgM83$^{+/-}$ mice. (B) The mean score of MBS. (C) Latency to fall from the rotarod. (D and E) Footprint analysis of the hindlimb stride length (D) and the hind-base width (E). (F and G) The average time to cross the beam (F) and the average number of side slip errors (G) on the beam. (H and I) T turn (H) and T total (I) of the pole test. (J and K) Average speed (J) and total distance (K) traveled during 15 minutes in the open field test. EUS-α-Syn PFFs TgM83$^{+/-}$ mice n = 12, DET-α-Syn PFFs TgM83$^{+/-}$ mice n = 20, EUS-PBS TgM83$^{+/-}$ mice n = 14, DET-PBS TgM83$^{+/-}$ mice n = 14. Data are the means ± SD. Statistical analysis was done by using the Student's t test and Mann-Whitney test, *P < 0.05.

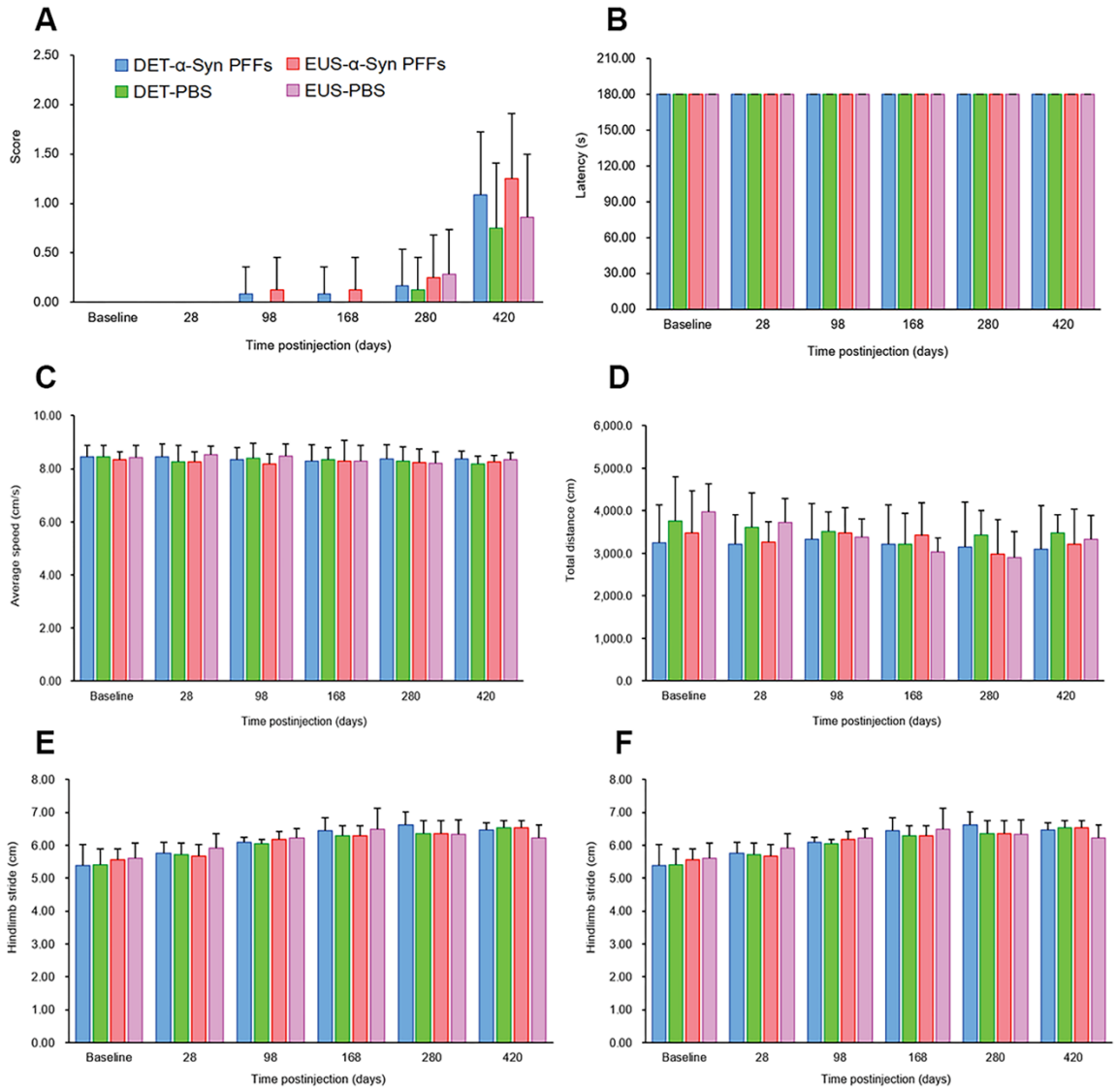

Figure S5. Behavioral analysis of C57BL/6 mice injected with human α-Syn PFFs. Related to Figure 4 and 5. (A) The mean score of MBS. (B) Latency to fall from the rotarod. (C and D) Average speed (C) and total distance (D) traveled during 15 minutes in the open field test. (E and F) Footprint analysis of the hindlimb stride length (E) and the hind-base width (F). EUS-α-Syn PFFs C57BL/6 mice n = 8, DET-α-Syn PFFs C57BL/6 mice n = 12, EUS-PBS C57BL/6 mice n = 7, DET-PBS C57BL/6 mice n = 8. Data are the mean ± SD. Statistical analysis was performed by using the Student's t test and Mann-Whitney test, n.s., non-significant.

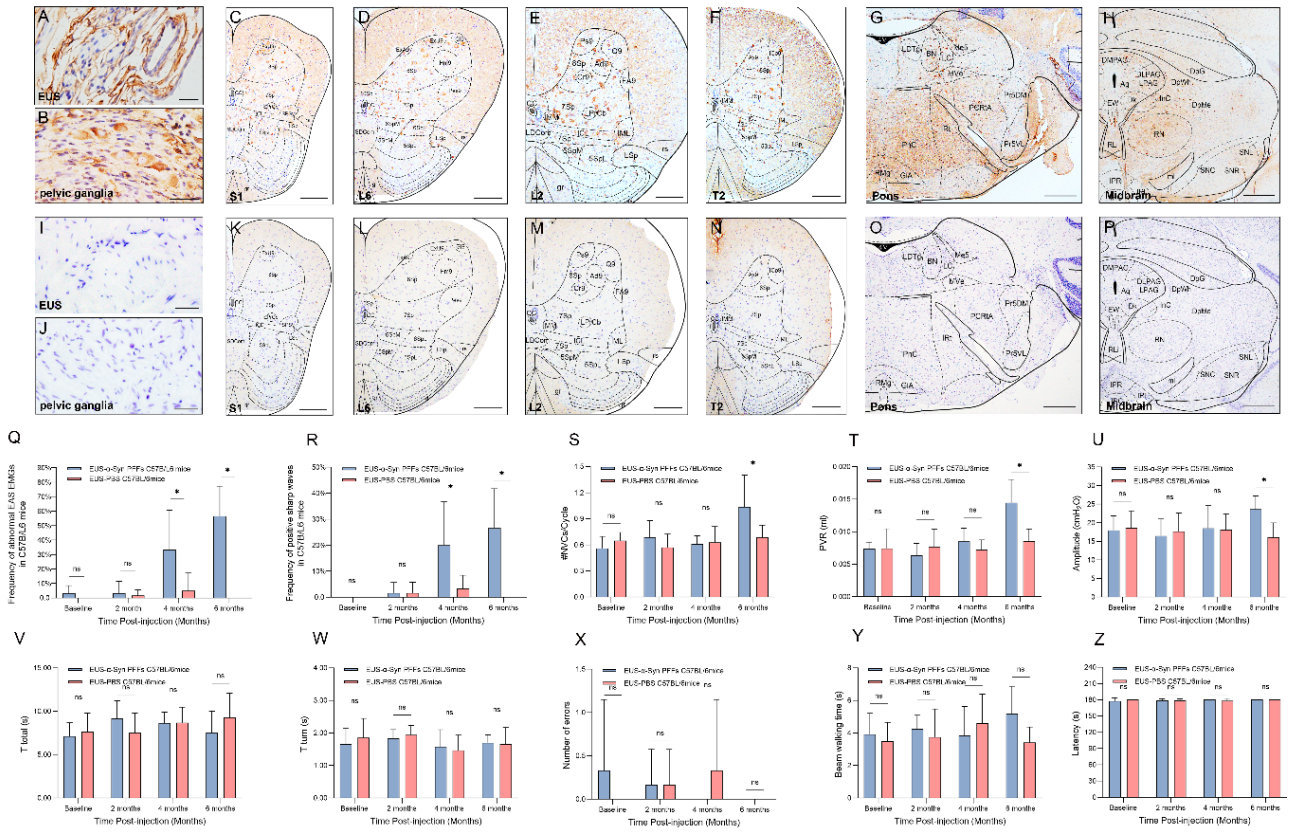

Figure S6. Related to Figure 2. (A-P) Representative immunohistochemical results of different segments from C57BL/6 mice injected with synthetic mouse α-Syn PFFs (A-H) and PBS (I-P) at 6 mpi. Pathological α-Syn was stained with anti-phospho-α-Syn (Ser 129) antibody. Representative images displayed the distribution of pα-Syn in EUS (A, I), pelvic ganglia (B, J), S1 (C, K), L6 (D, L), L2 (E, M), T2 (F, N), pons (G, O), and midbrain (H, P). [Scale bars, 40 μm (A, B, I, J); 250 μm (C-F, K-N); 1 mm (G, H, O, P).] (Q, R) Frequencies of abnormal EAS EMGs (Q) and positive sharp waves (R) in EUS-mouse α-Syn PFFs and PBS C57BL/6 mice. (S-U) Urodynamic evaluation for EUS-mouse α-Syn PFFs and PBS C57BL/6 mice including #NVCs/Cycle (S), PVR (T), and amplitude (U). (V-Z) Behavioral analysis of EUS-mouse α-Syn PFFs and PBS C57BL/6 mice. (V, W) T total (V) and T turn (W) of the pole test. (X, Y) The average number of side slip errors to cross the beam (X) and the average time (Y) on the beam. (Z) Latency to fall from the rotarod. n = 6 animals per group. Data are the means ± SD. Statistics was analyzed employing the Student's t test. *P < 0.05 indicates a significant difference between EUS-mouse α-Syn PFFs groups and PBS groups.

Supplemental Table

Table S1. Characteristics and the exam findings of patients. Related to Figure 1.

Age	Sex	Diagnosis	Duration (year)	MRI	UMSARS				Urodynamic examination†	Perianal electromyography†	α-synuclein filament in the bladder DET‡	α-synuclein filament in EUS§
					UMSARS I	UMSARS II	UMSARS III	UMSARS IV				
54	M	MSA-P	1.5	+	2	5	+	1	+	+	-	0
57	F	MSA-P	8	+	32	50	+	4	+	+	+	0
63	F	MSA-P	2	+	14	18	+	2	-	+	-	0
59	F	MSA-P	4	+	21	18	+	3	-	+	-	0
46	M	MSA-P	2	+	9	14	+	2	+	+	-	0
68	M	MSA-P	7	+	20	31	+	3	+	+	+	0
66	F	MSA-P	<1	+	7	12	+	1	-	+	+	0
70	F	MSA-P	3	+	32	46	+	4	+	+	+	0
66	F	MSA-P	3	+	18	24	+	3	+	+	-	+
72	F	MSA-P	5	+	34	42	+	4	+	+	+	+
63	M	MSA-P	2	+	7	13	+	2	+	-	-	+
64	F	MSA-P	7	+	33	42	+	5	+	+	+	+
59	F	MSA-P	4	+	18	15	+	4	+	-	+	+
59	M	MSA-C	2	+	10	13	+	2	+	+	+	0
50	M	MSA-C	1.5	+	2	3	+	1	-	-	-	0
47	M	MSA-C	8	+	30	21	+	4	+	+	+	0
63	F	MSA-C	2	+	21	14	+	1	+	-	-	0
50	M	MSA-C	2	+	5	6	+	1	+	-	-	0
61	M	MSA-C	3	+	20	18	+	4	+	+	+	0
61	M	MSA-C	5	+	8	9	+	2	+	+	+	0
51	F	MSA-C	3	+	8	6	+	1	-	+	-	0
58	F	MSA-C	3	+	4	5	+	2	+	+	-	0
50	F	MSA-C	2	+	12	14	+	2	+	+	+	0
64	F	MSA-C	2	+	14	24	+	4	+	+	+	0
62	F	MSA-C	3	+	14	18	+	3	+	+	+	0
64	M	MSA-C	3	+	10	11	+	2	+	+	+	0
64	F	MSA-C	3	+	30	12	+	4	+	-	-	+
52	F	MSA-C	8	+	33	22	+	5	+	+	+	+
53	F	MSA-C*	2	+	9	15	+	1	+	+	-	+
62	F	MSA-C	2	+	7	9	+	2	+	-	+	+
57	F	MSA-C	4	+	20	25	+	5	+	-	+	+
71	M	MSA-C	1	+	2	4	+	1	+	+	+	-
54	F	PD	10	-	NA				-	+	-	0
58	F	PD	3	-	NA				-	-	-	0
69	F	PD	10	-	NA				+	-	-	0
61	M	PD	6	-	NA				-	-	-	0
65	F	PD	10	-	NA				-	-	-	0
58	F	PD	4	-	NA				-	-	-	-
64	M	PD	8	-	NA				-	+	-	-
47	M	PSP	8	+	NA				-	-	-	0
69	M	PSP	3	+	NA				-	-	-	0
70	M	PSP	3	+	NA				-	-	-	0
69	F	PSP	3	+	NA				+	-	-	0
70	F	PSP-C	10	+	NA				-	-	-	0
67	M	PSP	4	+	NA				-	-	-	-

F, female; M, male; MSA-P, multiple system atrophy with predominant parkinsonism; MSA-C, multiple system atrophy with predominant cerebellar ataxia; PD, Parkinson's disease; PSP, progressive supranuclear palsy; PSP-C, progressive supranuclear palsy with predominant cerebellar ataxia; MRI, magnetic resonance imaging, including atrophy on MRI of putamen, middle cerebellar peduncle, pons, or cerebellum, -, absent; +, present; UMSARS, Unified Multiple System Atrophy Rating Scale (I. historical review of disease-related impairments; II. motor examination; III. autonomic examination, -, absent; +, present; IV. global disability scale); NA, not applicable.

*possible MSA-C.

†-, normal findings; +, abnormal findings.

‡ DET, detrusor; -, absent; +, present.

§ EUS, external urethral sphincter; -, absent; +, present; 0: not examined.

Transparent Methods

Patients

Forty-five patients (18 men, 27 women; age 60.6 ± 7.2 years) were enrolled consecutively from 2016 to 2018 with MSA (32 patients), PD (7 patients), or progressive supranuclear palsy (PSP) (6 patients) according to consensus criteria (Kalia and Lang, 2015; Litvan et al., 1996; Stefanova et al., 2009), respectively. In MSA, the phenotype was characterized by prevalently cerebellar signs in 19 patients and by parkinsonian signs in the remaining 13 patients. Disease severity was evaluated using Unified Multiple System Atrophy Rating Scale (UMSARS) (Low et al., 2015; Wenning et al., 2004). UMSARS Total is a sum of UMSARS Ⅰ and UMSARS Ⅱ. Demographic and clinical data are summarized in Table S1. At the time of enrollment, all subjects underwent clinical and electrophysiological evaluation as well as EUS and bladder biopsies at 3 sites: left wall, right wall, and triangle region (Figure 1J). Twenty subjects were also included in the study as controls (7 men, 13 women; age 58.5 ± 7.0 years). All biopsies were performed according to the outpatient procedures by experienced urologists in a prescriptive exam room. Cystoscopy was performed using standard cystoscope according to previously published procedures under local anesthesia with 1% xylocaine (Butros et al., 2015). The procedure was repeated until the EUS, left wall, right wall, and triangle region of bladder tissues were obtained. Samples were immediately fixed in 4% paraformaldehyde and kept at 4 °C for at least 2 days. All subjects provided informed consent for participation in the experiments. The study was executed with the approval of the Institutional Ethics Committees of the Zhengzhou University.

Urodynamic examination (UE) and external anal sphincter electromyography (EAS EMG) of patients

All human subjects underwent clinical and electrophysiological evaluation, including UE and EAS EMG, as previously described (Yamamoto et al., 2005; Yamamoto et al., 2014).

Animals

Male TgM83$^{+/-}$ expressing human A53T mutant α-Syn protein and male C57BL/6 as control mice were purchased from Nanjing Biomedical Research Institute of Nanjing University (Nanjing, China), and evaluated at the age of six to eight weeks. The hemizygous TgM83 mice expressed the human A53T α-Syn driven by the prion gene promoter (Giasson et al., 2002). C57BL/6 mice were chosen as the control mice because TgM83$^{+/-}$ mice were maintained on a mixed C57/C3H genetic background. Mice were kept in a near pathogen-free environment under standard conditions with food and water (21 °C, 12h/12h light-dark cycle). All experiments were conducted in accordance with the Guide for the Care and Use of Laboratory Animals. The protocols were approved by the Institutional Ethics Committees of the Zhengzhou University.

Surgery and retrograde tracing

To retrogradely label micturition reflex pathways, C57BL/6 and TgM83$^{+/-}$ mice were anesthetized with isoflurane inhalation (Prusiner et al., 2015), and 15 μl Fluoro-Gold (FG) (Fluorochrome, LLC, Denver, CO) was injected slowly into EUS or DET. Following the injections, the skin was sutured. After 14 days, mice were perfused as described before (Bácskai et al., 2014). The EUS or DET, pelvic ganglia, spinal cord and brain were removed and postfixed at 4 ℃ in a 30% sucrose solution containing 4% paraformaldehyde for at least 2 days. Serial transverse sections were cut at 20 μm using a freezing microtome (Leica CM1860 UV, Leica, Nussloch, Germany). Consecutive sections were collected, mounted, and cover-slipped with glycerol. Slides were then examined using an Olympus IX51 microscope equipped with epifluorescence.

α-Synuclein preformed fibrils (PFFs) preparation

Human α-Syn (S-1001, rPeptide) was resuspended in assembly buffer (20 mM Tris-HCl, 100 mM NaCl, pH 7.4) at concentration of 1 mg/ml. To obtain PFFs, the samples were placed in 2 ml sterile polypropylene tubes, sealed with parafilm, and agitated in a beaker with a magnetic stirrer (MS-H-Pro+, Scilogex, China) at 350 rpm for 7 days at 37 °C. After 7 days of incubation, the α-Syn fibrils were sonicated for 45 seconds using an ultrasonic cell disruptor at 10% of its peak amplitude (Scientz-IID, Ningbo, China). α-Syn fibrils were stored at -80 °C until use.

Transmission electron microscopy (TEM) imaging

The nature of the fibrillar α-Syn forms was assessed using Jeol 1400 (Jeol Ltd. Tokyo, Japan) TEM. First, a drop of fibrillar solution was transferred onto a carbon-coated 200-mesh grid and then negatively stained with 1% uranyl acetate. The images were recorded with Gatan Orius CCD camera (Gatan, Pleasanton, CA).

Modeling surgery

All injections were performed using a manual microinjector under an operating microscope. Mice were anesthetized with isoflurane inhalation and fixed in a supine position. After disinfection, mice were inoculated in the EUS with 15 μl α-Syn PFFs (48.89 ± 27.00 nm, 1 mg/ml) (Figure S1A-D) or phosphate buffered saline (PBS, Solarbio), or DET with 20 μl (1 mg/ml) α-Syn PFFs or PBS. The reason for selecting male mice is that the EUS boundary of male mice is clearer, making the injection more feasible. Following the injection, the exposed wound was sewn closed.

Immunohistochemical and double immunofluorescence staining

The paraffin-embedded tissues were cut into 4 μm thick sections with a Rotary Microtome (Leica RM2235, Leica, Nussloch, Germany). Immunohistochemistry and double-labeling immunofluorescence analysis were conducted as previously described by Luk et al. (Luk et al., 2012) using the following antibodies: phospho-α-synuclein (Ser 129) (mouse, Millipore, 1:800 or rabbit, Abcam, 1:600), α-synuclein filament (MJFR14) (rabbit, Abcam, 1:500), α-Syn aggregates (5G4) (mouse, Millipore, 1:800), ubiquitin (rabbit, Cell Signaling Technology, 1:400), Iba-1 (rabbit, Wako, 1:400), myelin basic protein (rabbit, Abcam, 1:900), neurofilament heavy polypeptide (mouse, Abcam, 1:600), anti-tyrosine hydroxylase (TH) (rabbit, Abcam, 1:600), glial fibrillary acidic protein (GFAP) (rabbit, Abcam, 1:600), microtubule-associated protein-2 (MAP-2) (rabbit, Abcam, 1:800), calbindin-D28k (rabbit, Abcam, 1:1000), Rhodamine Red™-X (RRX) AffiniPure donkey anti-mouse IgG (H+L) (donkey, Jackson ImmunoResearch, 1:400), Cy™2 AffiniPure donkey anti-rabbit IgG (H+L) (donkey, Jackson ImmunoResearch, 1:400). Cell nuclei were stained using Hoechst33258 (1:1000, Solarbio). Slides were coverslipped with

glycerol. Digital images were captured using Olympus IX51 microscope mounted with DP71 Olympus digital camera. Photoshop CS6 (Adobe Systems) was used to assemble montages.

We used 20 EUS-α-Syn PFFs TgM83$^{+/-}$ mice and 10 EUS-PBS TgM83$^{+/-}$ mice for statistical analysis of immunostaining. Calbindin-D28K-positive neurons and MAP-2-positive neurons were counted to evaluate the number of neurons. Mean optical density of MAP-2 was measured to evaluate the size of neurons using the ImageJ software (US National Institutes of Health). Mean optical density of MBP and GFAP was measured to evaluate demyelination and astrogliosis, respectively. The Pearson's correlation and the Mander's colocalization coefficients were measured to quantify the colocalization of ubiquitin with pα-Syn and TH using the ImageJ software. DET, EUS, pelvic ganglia, and serial coronal sections of the spinal cord, pons, midbrain, and cerebellum were analyzed, especially the representative sections of spinal cord (S1, L6, L2, T2), pons (Bregma -5.40 mm), midbrain (Bregma -3.16 mm), and cerebellum (Bregma -5.88 mm). The quantification and statistical analysis of the immunohistological results for each animal were conducted using the representative sections in a slide.

Tissue preparation

RIPA-insoluble fractions were prepared. Firstly, tissues were homogenized in TBS+ (50 mM Tris-HCl, pH 7.4, 175 mM NaCl; 5 mM EDTA, protease inhibitor cocktails). Then the homogenates were spun for 30 minutes at 120000 g and divided into soluble components and pellets. The soluble component refers to the supernatant after above step that does not contain α-Syn inclusions. The pallets contain most α-Syn inclusions. The pellets were subsequently extracted in TBS+ containing 1% Triton X-100, TBS+ containing 1M sucrose, and RIPA buffer, sequentially, and each extraction step was followed by centrifugation for 20 minutes at 12000g. After all these steps, we obtained the RIPA-insoluble pellets containing phosphorylated α-Syn (pα-Syn) inclusions. Then the RIPA-insoluble pellets were solubilized in 8 M urea/5% SDS for subsequent detection.

Sarkosyl-insoluble fractions were also prepared as previously described (Masuda-Suzukake et al., 2014). Firstly, tissues were homogenized in TBS+ (10 mM Tris-HCl, pH 7.4, 175 mM NaCl; 5 mM EDTA, protease inhibitor cocktails). Then the homogenates

were spun for 30 minutes at 120000g and divided into soluble components and pellets. The pellets were subsequently extracted in TBS+ containing 1% Triton X-100, and TBS+ containing 1% sarkosyl, sequentially, and each extraction step was followed by centrifugation for 20 minutes at 12000g. Then the sarkosyl-insoluble was solubilized in 30 mM Tris–HCl, pH 7.4 for subsequent detection.

Western blotting analysis

After mice were anesthetized and decapitated, the spinal cord and several brain regions such as PAG, RN, pons, and cerebellum were separated on a cold stage. The isolated mice tissues were then stored in liquid nitrogen for further treatment. The transferred polyvinylidene fluoride (PVDF) membranes for the Western blotting as previously described (Kohl et al., 2016) were incubated with phospho-α-synuclein (Ser 129) antibody (mouse, Millipore, 1:1200 or rabbit, Abcam, 1:1000). Forty-eight hours later, the membranes were washed in TBST (TBS with 0.1% Tween-20) and incubated with HRP-conjugated goat anti-mouse or goat anti-rabbit secondary antibodies for 2 hours at room temperature and visualized with enhanced chemiluminescence (Thermo Fisher Scientific). Proteins' densities on the blots were normalized against those of GAPDH. All immunoreactive bands from Western blotting analysis were quantified by pixel intensity using FluorChem 8900 software (Alpha Innotech, San Leandro, CA, USA). The relative pα-Syn level was measured by the ratio of the pixel intensity of the pα-Syn band to the pixel intensity of the corresponding GAPDH band.

EAS EMG

EAS EMG was carried out in all animals before injection for control groups and at correspondingly post-injection times to determine EAS denervation-reinnervation. Animals in each group underwent EAS EMG as follows (Aghaee-Afshar et al., 2009; Buffini et al., 2012; Healy et al., 2008; Lane et al., 2013): anesthesia was induced using isoflurane inhalation. Limb withdrawal to paw pinch and corneal reflexes of animals were observed to assess the level of anesthesia. After placing the animal supine, shaving the thigh, and establishing a ground connection, a disposable concentric 30-gauge needle electrode (Technomed Europe), which has a 25-mm length, 0.30-mm diameter, and

0.021-mm^2 recording area, was inserted at the 3 or 9 o'clock position of the anal orifice perpendicularly into the EAS from the perianal skin close to the mucocutaneous junction to a depth of approximately 1 to 2 mm. The point of the electrode insertion was adjusted under audio guidance until a permanent tonic activity was recorded, in order to ensure that the electrode has entered EAS. If the mouse discharged a fecal pellet during the recording process, a pair of forceps were used to gently clip it out. EMG was performed with an EMG monitoring machine (MEB-2306C, NIHON KOHDEN CORPORATION, Tokyo, Japan) at a sweep speed of 10 ms/div and a gain of 100 uv/div. Abnormal EAS EMGs were simultaneously visualized and recorded. EMG activity was quantified by frequency of abnormal EAS EMGs (fibrillation potentials, positive sharp waves, complex repetitive discharges (CRD), fasciculation potentials, myokymic discharges, and satellite potential) in each group (Daube and Rubin, 2009; Palace et al., 1997; Schwarz et al., 1997). Frequency of positive sharp waves in different groups was also separately analyzed.

Cystometry evaluations

All animals were subjected to cystometric experiment to evaluate their urinary function before injection and at corresponding time points of post-injection following the methods reported previously (Boudes et al., 2013; Fandel et al., 2016; Girard et al., 2012; Silva et al., 2015). The animal was put supine and the bladder was exposed via a lower midline abdominal incision under isoflurane anesthesia. A polyethylene catheter-50 (Clay-Adams, Parsippany, New Jersey, USA) was implanted into the apical bladder dome and secured in place with a 6/0 purse-string sutures (Ethicon, Noderstedt, Germany). We flushed the catheter with saline to ensure no leakage and then threaded it from neck to the lower back through the subcutaneous tunnel anchored to the neck skin, finally closed the abdominal wall and skin. Through a three-way tap, the bladder catheter was connected to an infusion pump (B. Braun Sharing Expertise, Germany) and a pressure transducer (AD Instruments, Castle Hill, New South Wales, Australia) coupled to a computerized BL-420S data acquisition and analysis system (Techman Soft, Chengdu, China) which amplified and recorded intravesical pressure from the pressure transducer. We applied a heating lamp and room-temperature saline to maintain the body

temperature of mice. Bladders were given a continuous infusion of 0.9% NaCl at a constant rate (20 μl/min) and after an equilibration period of 20-30 minutes, the intravesical pressure was recorded and voiding events were observed and noted for 30 minutes.

The following urodynamic parameters (Boudes et al., 2013; Fandel et al., 2016; Girard et al., 2012; Lee et al., 2013; Silva et al., 2015) were used for the current study: (1) Maximum voiding pressure (P_{max}; cmH_2O); (2) Basal bladder pressure (BBP; cmH_2O): the lowest bladder pressure during filling phase; (3) Amplitude (cmH_2O): P_{max} - BBP; (4) Bladder leak point pressure (BLPP; cmH_2O): intravesical pressure recorded at the first leaking/micturition point; (5) Threshold pressure (Pt; cmH_2O); (6) Nonvoiding contractions during filling phase (NVCs): rhythmic intravesical pressure rises (> 5 cmH_2O from baseline pressure) without any fluid leakage from the urethra; (7) Postvoid residual volume (PVR; ml): the remaining saline in the bladder collected and measured after stopping the infusion at the end of the final micturition cycle; (8) Maximum bladder capacity (MBC; ml): volume between the start of infusion and the BLPP; (9) Voided volume (VV; ml): MBC - PVR; (10) Intercontraction interval (ICI; s).

Behavioral test

To evaluate α-Syn PFFs-induced behavioral deficits, mice were assessed by the following tests. TgM83$^{+/-}$ and C57BL/6 mice were tested every 7 days starting from 2 mpi. Blinded experiments were performed to treatment group for all behavioral tests.

The motor behavioral scale (MBS)

MBS was used as Fernagut et al. previously reported (Fernagut et al., 2002). Higher score indicated higher disability and the maximum total score was 10. The total score was determined and used for the statistical analysis.

Rotarod test

Motor coordination was assessed following the method previously reported by Duclot et al. (Duclot et al., 2012) with modifications. In brief, a rotating rod (Rotarod YLS-4C; YiYan Science and Technology Development Co. Ltd., Shandong, China) was used. At each

time point, mice were placed on the rod rotating at 30 rpm. The latency to fall off the rotarod within the maximum time (180 seconds) was recorded, if a mouse stayed on the rod until the end of the 3 minutes, a time of 180 seconds was recorded. Mice received three trials per day with a 15-minute inter-trial interval. The mean latency to fall off the rotarod was statistically analyzed.

Open field test

To assess general activity, locomotion, and anxiety of the mice, the open field test system (Wuhan YiHong Sci. & Tech.Co. Ltd.) was applied. Mice were placed in the center of the open field (37.5 × 37.5 × 34.8 cm) and tested for 15 minutes at the same time of the day (6:00 p.m. to 9:00 p.m.). Activity was analyzed by the Anilab software version 5.10, registered version (Anilab Software & Instruments Co., Ltd., China). At the end of testing, the arena was cleaned with 75% alcohol to remove olfactory cues. The tests were performed in a dark room that was isolated from external noises and light during the test period. Total distance (cm), average speed (cm/s), and zone crossing were statistically analyzed.

Footprint test

The footprint test was performed to examine the gait of the mice. Paws of the mice were painted with water-soluble non-toxic paint of different colors (fore-paws in red and hind-paws in green). The animals were then allowed to walk along a restricted cardboard tunnel (50 cm long, 5 cm wide, 10 cm high) into an enclosed box and a sheet of white paper (42 cm long, 4.5 cm wide) was placed on the floor of the tunnel, and one set of footprints was collected for each animal. Three steps from the middle portion of each run were measured for four parameters (cm): (1) stride length (front and hind legs). (2) The front- and hind-base width. The mean of each set of values was statistically analyzed (Stefanova et al., 2005).

Beam walking test

Balance and bradykinesia were assessed with the method described before with modifications (Schafferer et al., 2016). The beams consisted of two different types of

wood (each measuring 80 cm long, one was 1.6 cm, and the other 0.9 cm wide) placed horizontally 50 cm above the floor, respectively. Two daily sessions of three trials were performed using the 1.6 cm width large beam during training. Mice were then tested using the 0.9 cm width beam. Mice were allowed to perform in three consecutive trials. The time for traversing 50 cm as well as the number of sideslip errors were recorded on each trial. The average traverse duration and average number of sideslip errors of the three trials were statistically analyzed.

Pole test

The pole test was performed to assess motor coordination and balance. A vertical gauze-taped pole (1 cm diameter, 50 cm height) with a small cork ball (3 cm diameter) at the top was applied. Mice were placed with their head upward right below the ball. The time taken to turn completely downward (T turn) and total time taken to reach the base of the pole with four paws (T total) were recorded. The maximum cutoff of total time to stop this test was 120 seconds. This test was performed three times for each mouse, while the average time was statistically analyzed (Zhou et al., 2016).

Statistical analysis

All statistical analyses of data were performed using SPSS 21.0 (IBM, Armonk, New York, USA) and Prism software 8.0 (GraphPad Software, La Jolla, CA). Data from immunohistochemistry, immunofluorescence, and negative-stained transmission electron micrographs were analyzed by ImageJ software (US National Institutes of Health). Characteristics of patients were presented as mean ± standard deviation (SD), statistical differences among groups of subjects were assessed using the one-way ANOVA. Histopathological parameters of mice were analyzed using Student's t test. Additionally, behavioral data and cystometry parameters of mice were presented as mean ± SD, employing Student's t test for comparison between two groups while one-way ANOVA for three when these data were distributed normally ($P > 0.05$ by Shapiro-Wilk test). Otherwise, the Mann-Whitney test was used for two groups versus Kruskal-Wallis test for three. Frequencies of abnormal EAS EMGs and positive sharp waves in different groups

were presented as mean ± standard error of mean (SEM) and statistically analyzed using the one-way ANOVA. P-values < 0.05 were considered to be statistically significant.

Supplemental References

Aghaee-Afshar, M., Rezazadehkermani, M., Asadi, A., Malekpour-Afshar, R., Shahesmaeili, A., and Nematollahi-mahani, S.N. (2009). Potential of human umbilical cord matrix and rabbit bone marrow-derived mesenchymal stem cells in repair of surgically incised rabbit external anal sphincter. Diseases of the colon and rectum *52*, 1753-1761.

Bácskai, T., Rusznák, Z., Paxinos, G., and Watson, C. (2014). Musculotopic organization of the motor neurons supplying the mouse hindlimb muscles: a quantitative study using Fluoro-Gold retrograde tracing. Brain structure & function *219*, 303-321.

Boudes, M., Uvin, P., Pinto, S., Voets, T., Fowler, C.J., Wenning, G.K., De Ridder, D., and Stefanova, N. (2013). Bladder dysfunction in a transgenic mouse model of multiple system atrophy. Movement disorders : official journal of the Movement Disorder Society *28*, 347-355.

Buffini, M., O'Halloran, K.D., O'Herlihy, C., O'Connell, P.R., and Jones, J.F. (2012). Comparison of the motor discharge to the voluntary sphincters of continence in the rat. Neurogastroenterology and motility : the official journal of the European Gastrointestinal Motility Society *24*, e175-184.

Butros, S.R., McCarthy, C.J., Karaosmanoglu, A.D., Shenoy-Bhangle, A.S., and Arellano, R.S. (2015). Feasibility and effectiveness of image-guided percutaneous biopsy of the urinary bladder. Abdominal imaging *40*, 1838-1842.

Daube, J.R., and Rubin, D.I. (2009). Needle electromyography. Muscle & nerve *39*, 244-270.

Duclot, F., Lapierre, M., Fritsch, S., White, R., Parker, M.G., Maurice, T., and Cavailles, V. (2012). Cognitive impairments in adult mice with constitutive inactivation of RIP140 gene expression. Genes, brain, and behavior *11*, 69-78.

Fandel, T.M., Trivedi, A., Nicholas, C.R., Zhang, H., Chen, J., Martinez, A.F., Noble-Haeusslein, L.J., and Kriegstein, A.R. (2016). Transplanted Human Stem Cell-Derived Interneuron Precursors Mitigate Mouse Bladder Dysfunction and Central Neuropathic Pain after Spinal Cord Injury. Cell stem cell *19*, 544-557.

Fernagut, P.O., Diguet, E., Stefanova, N., Biran, M., Wenning, G.K., Canioni, P., Bioulac, B., and Tison, F. (2002). Subacute systemic 3-nitropropionic acid intoxication induces a distinct motor disorder in adult C57Bl/6 mice: behavioural and histopathological characterisation. Neuroscience *114*, 1005-1017.

Giasson, B.I., Duda, J.E., Quinn, S.M., Zhang, B., Trojanowski, J.Q., and Lee, V.M. (2002). Neuronal alpha-synucleinopathy with severe movement disorder in mice expressing A53T human alpha-synuclein. Neuron *34*, 521-533.

Girard, B.M., Tompkins, J.D., Parsons, R.L., May, V., and Vizzard, M.A. (2012). Effects of CYP-induced cystitis on PACAP/VIP and receptor expression in micturition pathways and bladder function in mice with overexpression of NGF in urothelium. Journal of molecular neuroscience : MN *48*, 730-743.

Healy, C.F., O'Herlihy, C., O'Brien, C., O'Connell, P.R., and Jones, J.F. (2008). Experimental models of neuropathic fecal incontinence: an animal model of childbirth injury to the pudendal nerve and external anal sphincter. Diseases of the colon and rectum *51*, 1619-1626; discussion 1626.

Kalia, L.V., and Lang, A.E. (2015). Parkinson's disease. Lancet (London, England) *386*, 896-912.

Kohl, Z., Ben Abdallah, N., Vogelgsang, J., Tischer, L., Deusser, J., Amato, D., Anderson, S., Muller, C.P., Riess, O., Masliah, E.*, et al.* (2016). Severely impaired hippocampal neurogenesis associates with an early serotonergic deficit in a BAC alpha-synuclein transgenic rat model of Parkinson's disease. Neurobiology of disease *85*, 206-217.

Lane, F.L., Jacobs, S.A., Craig, J.B., Nistor, G., Markle, D., Noblett, K.L., Osann, K., and Keirstead, H. (2013). In vivo recovery of the injured anal sphincter after repair and injection of myogenic stem cells: an experimental model. Diseases of the colon and rectum *56*, 1290-1297.

Lee, Y.S., Lin, C.Y., Jiang, H.H., Depaul, M., Lin, V.W., and Silver, J. (2013). Nerve regeneration restores supraspinal control of bladder function after complete spinal cord injury. The Journal of neuroscience : the official journal of the Society for Neuroscience *33*, 10591-10606.

Litvan, I., Agid, Y., Calne, D., Campbell, G., Dubois, B., Duvoisin, R.C., Goetz, C.G., Golbe, L.I., Grafman, J., Growdon, J.H.*, et al.* (1996). Clinical research criteria for the diagnosis of progressive supranuclear palsy (Steele-Richardson-Olszewski syndrome): report of the NINDS-SPSP international workshop. Neurology *47*, 1-9.

Low, P.A., Reich, S.G., Jankovic, J., Shults, C.W., Stern, M.B., Novak, P., Tanner, C.M., Gilman, S., Marshall, F.J., Wooten, F., *et al.* (2015). Natural history of multiple system atrophy in the USA: a prospective cohort study. The Lancet Neurology *14*, 710-719.

Luk, K.C., Kehm, V.M., Zhang, B., O'Brien, P., Trojanowski, J.Q., and Lee, V.M. (2012). Intracerebral inoculation of pathological alpha-synuclein initiates a rapidly progressive neurodegenerative alpha-synucleinopathy in mice. The Journal of experimental medicine *209*, 975-986.

Masuda-Suzukake, M., Nonaka, T., Hosokawa, M., Kubo, M., Shimozawa, A., Akiyama, H., and Hasegawa, M. (2014). Pathological alpha-synuclein propagates through neural networks. Acta neuropathologica communications *2*, 88.

Palace, J., Chandiramani, V.A., and Fowler, C.J. (1997). Value of sphincter electromyography in the diagnosis of multiple system atrophy. Muscle & nerve *20*, 1396-1403.

Prusiner, S.B., Woerman, A.L., Mordes, D.A., Watts, J.C., Rampersaud, R., Berry, D.B., Patel, S., Oehler, A., Lowe, J.K., Kravitz, S.N., *et al.* (2015). Evidence for α-synuclein prions causing multiple system atrophy in humans with parkinsonism. Proc Natl Acad Sci U S A *112*, E5308-5317.

Schafferer, S., Khurana, R., Refolo, V., Venezia, S., Sturm, E., Piatti, P., Hechenberger, C., Hackl, H., Kessler, R., Willi, M., *et al.* (2016). Changes in the miRNA-mRNA Regulatory Network Precede Motor Symptoms in a Mouse Model of Multiple System Atrophy: Clinical Implications. PloS one *11*, e0150705.

Schwarz, J., Kornhuber, M., Bischoff, C., and Straube, A. (1997). Electromyography of the external anal sphincter in patients with Parkinson's disease and multiple system atrophy: frequency of abnormal spontaneous activity and polyphasic motor unit potentials. Muscle & nerve *20*, 1167-1172.

Silva, R.B., Sperotto, N.D., Andrade, E.L., Pereira, T.C., Leite, C.E., de Souza, A.H., Bogo, M.R., Morrone, F.B., Gomez, M.V., and Campos, M.M. (2015). Spinal blockage of P/Q- or N-type voltage-gated calcium channels modulates functional and symptomatic changes related to haemorrhagic cystitis in mice. British journal of pharmacology *172*, 924-939.

Stefanova, N., Bucke, P., Duerr, S., and Wenning, G.K. (2009). Multiple system atrophy: an update. The Lancet Neurology *8*, 1172-1178.

Stefanova, N., Reindl, M., Neumann, M., Haass, C., Poewe, W., Kahle, P.J., and Wenning, G.K. (2005). Oxidative stress in transgenic mice with oligodendroglial alpha-synuclein overexpression replicates the characteristic neuropathology of multiple system atrophy. The American journal of pathology *166*, 869-876.

Wenning, G.K., Tison, F., Seppi, K., Sampaio, C., Diem, A., Yekhlef, F., Ghorayeb, I., Ory, F., Galitzky, M., Scaravilli, T., *et al.* (2004). Development and validation of the Unified Multiple System Atrophy Rating Scale (UMSARS). Movement disorders : official journal of the Movement Disorder Society *19*, 1391-1402.

Yamamoto, T., Sakakibara, R., Uchiyama, T., Liu, Z., Ito, T., Awa, Y., Yamamoto, K., Kinou, M., Yamanishi, T., and Hattori, T. (2005). When is Onuf's nucleus involved in multiple system atrophy? A sphincter electromyography study. Journal of neurology, neurosurgery, and psychiatry *76*, 1645-1648.

Yamamoto, T., Sakakibara, R., Uchiyama, T., Yamaguchi, C., Ohno, S., Nomura, F., Yanagisawa, M., Hattori, T., and Kuwabara, S. (2014). Time-dependent changes and gender differences in urinary dysfunction in patients with multiple system atrophy. Neurourology and urodynamics *33*, 516-523.

Zhou, T., Zu, G., Zhang, X., Wang, X., Li, S., Gong, X., Liang, Z., and Zhao, J. (2016). Neuroprotective effects of ginsenoside Rg1 through the Wnt/beta-catenin signaling pathway in both in vivo and in vitro models of Parkinson's disease. Neuropharmacology *101*, 480-489.